residual virus and the plant extract were removed, and cells were refed with fresh medium containing the plant extract for 46 hours. As shown in Table 2, ethanol extracts of TSL and MLL showed anti-HCV activities at both the entry and post-entry steps. On the other hand, MMS and FFL exhibited anti-HCV activities principally at the entry step.

To further confirm anti-HCV activities of the extracts of TSL, MLL, MMS and FFL, we investigated whether those extracts (30 μg/ml) affect HCV protein expression level, HCV RNA replication and infectious virus production in HCV J6/JFH1-P47-infected cells. The results showed that treatment with TSL and MLL markedly decreased the amounts of the HCV NS3 protein while that with MMS and FFL to lesser extents (Figure 2A). To quantitate the effect of TSL, MLL, MMS and FFL more accurately, we measured HCV RNA levels by real-time quantitative RT-PCR. Again, TSL and MLL markedly suppressed HCV RNA levels while MMS and FFL to lesser extents (Figure 2B). Moreover, TSL and MLL markedly inhibited the infectious virus production by >1 $\log_{10}$, FFL by 1 $\log_{10}$ while MMS to a lesser extent of <1 $\log_{10}$ (Figure 2C and 2D).

Antiviral activities of ethanol extracts of TSL, MLL, MMS and FFL against HCV genotypes 1 to 7

Antiviral activities of the extracts of TSL, MLL, MMS and FFL were further examined for other HCV strains of various genotypes. First, we examined the HCV J6/JFH1-P1 (passage 1) strain [15] and found that TSL, MLL, MMS and FFL inhibited HCV J6/JFH1-P1 infection with IC_{50} of 2.0, 2.1, 6.2 and 5.7 μg/ml, respectively. Dose-dependent anti-HCV activities of those extracts against the HCV J6/JFH1-P1 were shown in Figure 1B. We then compared anti-HCV activities of those plant extracts (30 μg/ml) using other HCV genotypes, including 1a to 7a, 1b and 2b [3] along with the JFH1 strain of genotype 2a [16]. The results showed that TSL and MLL exerted antiviral activities against all the HCV strains tested almost to the same extent (Table 3). On the other hand, MMS exhibited significantly weaker antiviral activities against the J8/JFH1 and QC69/JFH1 strains of genotypes 2b and 7a, respectively, compared to the other HCV strains. Notably, FFL at the concentration of 30 μg/ml did not exert detectable antiviral activities against the H77C/JFH1 strain of genotype 1a while exhibiting >90% inhibition at the same concentration against all the other HCV strains tested.

Discussion

A wide variety of traditional medicinal plants and herbs were reported to have antiviral activities against various viruses. In this study we analyzed anti-HCV activities of ethanol extracts of 21 medicinal plants that belong to 17 different species explored in the East Java region, Indonesia. In the initial screening, we used the HCV J6/JFH1-P47 strain as it is highly adapted to the Huh7.5 cell culture system [14] and, therefore, was easier to apply for the screening of many samples than the original P1 strain. Once we found possible candidates with anti-HCV activities, we used the original J6/JFH1-P1 strain to confirm the results.

Of the 21 samples, *T. sureni* leave (TSL), *M. latifolia* leave (MLL), *M. multiglandulosa* stem (MMS) and *F. fistulosa* leaves (FFL) were found to possess significant anti-HCV activities with IC_{50} of 13.9, 3.5, 17.1 and 15.0 μg/ml, respectively, against the J6/JFH1-P47 strain of HCV genotype 2a (Table 1 and Figure 1A), and 2.0, 2.1, 6.2 and 5.7 μg/ml, respectively, against the J6/JFH1-P1 strain (Figure 1B). We further examined anti-HCV activities of those plant extracts against other HCV genotypes, including 1a to 7a, 1b and 2b [3]. Although most of the HCV strains of different genotypes tested were inhibited by those plant extracts, there were some exceptions; the H77C/JFH1 strain (genotype 1a) showed significant resistance to FFL, and the J8/JFH1 (2b) and QC69/JFH1 strains (7a) to MMS to a lesser extent

Table 2 Mode of action of ethanol extracts of *T. sureni* leaves (TSL), *M. latifolia* leaves (MLL), *M. multiglandulosa* stem (MMS) and *F. fistulosa* leaves (FFL)

Plant extract	% Inhibition[a]			Mode of action
	During + Post inoculation	During inoculation	Post inoculation	
T. sureni leaves (TSL)	97.2 ± 1.3[b]	92.2 ± 2.2	60.9 ± 2.2	Entry inhibition
				Post-entry inhibition
M. latifolia leaves (MLL)	98 ± 0.3	90.8 ± 0.2	60.6 ± 4.9	Entry inhibition
				Post-entry inhibition
M. multiglandulosa stem (MMS)	86.6 ± 1.4	73 ± 0.9	33.5 ± 1.4	Entry inhibition
F.fistulosa leaves (FFL)	93.8 ± 1.3	86.7 ± 3.1	20.5 ± 2.6	Entry inhibition

[a]% Inhibition at the concentration of 30 μg/ml.
[b]Data represent means ± SEM of data from two independent experiments using HCV J6/JFH1-P47.

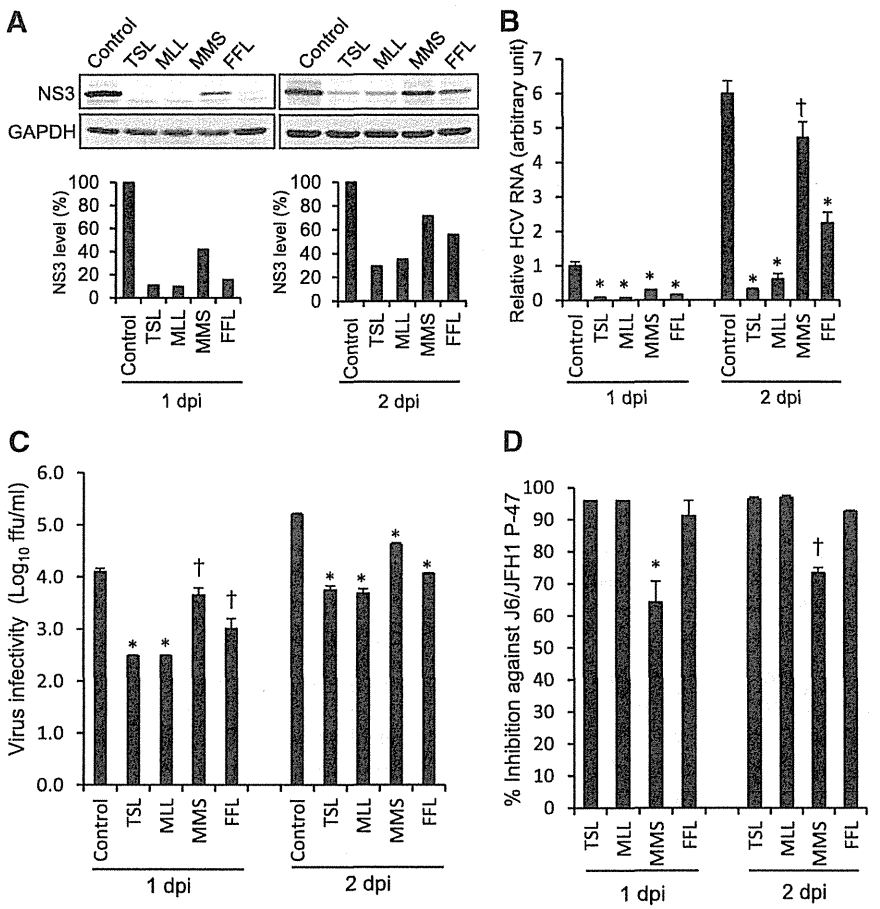

Figure 2 Inhibition of HCV protein expression, HCV RNA replication and infectious virus production by ethanol extracts of TSL, MLL, MMS and FFL. (A) Huh 7.5 cells infected with HCV J6/JFH1-P47 and treated with the extracts (30 μg/ml) of TSL, MLL, MMS and FFL (see Figure 1A) and the untreated control were subjected to Western blot analysis using monoclonal antibody against the HCV NS3 protein at 1 and 2 days post-infection (dpi). GAPDH served as an internal control to verify equal amounts of sample loading. Signal intensities of NS3 were normalized to the corresponding GAPDH signal. **(B)** Amounts of HCV RNA in the cells described in **(A)** were measured by real-time quantitative RT-PCR analysis. The HCV RNA amounts were normalized to GAPDH mRNA expression levels. Data represent means ± SEM of data from two independent experiments, and the value for the untreated control at 1 dpi was arbitrarily expressed as 1.0. *, $P < 0.000001$; ǂ, $P < 0.001$, compared with the control. **(C)** Virus infectivity in the culture supernatants of the cells described in (A) was measured. Data represent means ± SEM of data from two independent experiments. ǂ, $P < 0.05$; *, $P < 0.005$, compared with the control. **(D)** Inhibition of HCV infectivity by the extracts (30 μg/ml) of TSL, MLL, MMS and FFL are shown. *, $P < 0.05$; ǂ, $P < 0.01$, compared with TSL.

(Table 3). The difference in the amino acid sequences of the viral envelope proteins, especially E2, is likely to account for the different degree of the inhibition by a given extract among different HCV strains.

In this study we have not yet isolated a compound responsible for the anti-HCV activities; the study is still under way. It was reported that a methanol extract of *T. sureni*, a plant from Meliaceae family, showed antiviral activities against herpes simplex virus type 1 (HSV-1) with IC_{50} of 37 μg/ml [17]. By activity-guided fractionation and subsequent structure determination, the authors found that tannic acid and methyl and ethyl gallic acids possessed anti-HSV-1 activities with IC_{50} of 32, 20 and 26 μg/ml, respectively. Those compounds are known to bind to viral surface proteins to inhibit the virus infectivity, thereby exhibiting antiviral activities at the entry step. There have been no reports to date on the anti-HCV activities of *T. sureni* extracts, including TSL.

Chemical compounds of *M. latifolia, M. multiglandulosa* and *F. fistulosa* that possess antiviral activities have not been reported yet. An ethyl acetate extract of *M. vitiflora*, a plant genetically close to *M. latifolia*, was reported to possess antibacterial activities against methicillin-resistant *Staphylococcus aures* and *Micrococcus luteus* [18]. The authors identified some compounds contained in the extract,

Table 3 Antiviral activities of ethanol extracts of *T. sureni* leaves (TSL), *M. latifolia* leaves (MLL), *M. multiglandulosa* stem (MMS) and *F.fistulosa* leaves (FFL) against various HCV strains of different genotypes

HCV strain (genotype)	% Inhibition[a]			
	T. sureni leaves (TSL)	*M. latifolia* leaves (MLL)	*M. multiglandulosa* stem (MMS)	*F. fistulosa* leaves (FFL)
J6/JFH1 P47 (2a)	97.2 ± 1.3[b]	98.0 ± 0.3	86.7 ± 1.4	93.8 ± 1.3
J6/JFH1 (2a)	98.5 ± 2.1	99.5 ± 0.7	73.2 ± 2.1	96.1 ± 1.4
JFH1 (2a)	100 ± 0.0	100.0 ± 0.0	67.3 ± 8.2	92.3 ± 0.0
H77C/JFH1 (1a)	98.2 ± 2.5	100.0 ± 0.0	83.9 ± 2.5	**5.4 ± 2.5[c]**
J4/JFH1 (1b)	79.2 ± 11.8	91.7 ± 5.9	72.9 ± 8.8	93.8 ± 2.9
J8/JFH1 (2b)	100.0 ± 0.0	100.0 ± 0.0	**34.4 ± 13.3[c]**	93.8 ± 0.0
S52/JFH1 (3a)	97.8 ± 3.1	100.0 ± 0.0	95.6 ± 3.1	97.8 ± 0.0
ED43/JFH1 (4a)	94.2 ± 1.2	98.3 ± 0.0	59.5 ± 1.2	97.5 ± 1.2
SA13/JFH1 (5a)	100.0 ± 0.0	96.1 ± 1.1	89.8 ± 1.1	93.8 ± 2.2
HK6a/JFH1 (6a)	100.0 ± 0.0	91.2 ± 4.2	67.6 ± 20.8	91.2 ± 4.2
QC69/JFH1 (7a)	100.0 ± 0.0	87.0 ± 6.1	**39.1 ± 0.0[c]**	95.7 ± 6.1

[a]% Inhibition at the concentration of 30 μg/ml.
[b]Data represent means ± SEM of data from two independent experiments using HCV J6/JFH1-P47.
[c]% Inhibition of <40% are written in boldface letters.

including coumarin and terpenoid compounds. Other Melicope species have been investigated for their chemical compounds. *M. triphylla* leaves were reported to contain 15 flavonoid compounds. Recently, Higa et al. [19] reported five flavonoids isolated from *M. triphylla* leaves; 5,8-dihydroxy-3,7dimethoxy-3,4-methylenedioxyflavone, 7-hydroxy-3,5-di-methoxy-3',4'-methylenedioxyflavone, 7-(2,3-dihydroxy-3-methylbutoxy)-3,5-dimethoxy-3',4'-methylene-dioxyflavone, 7-(2,3-dihydroxy-3-methylbutoxy)-3-3',4',5-tetramethoxyflavone, and 7-(2,3-dihydroxy-3-methylbutoxy)-3,3'4',5,8-pentamethoxyflavone. There have been no reports to date on the antiviral activities of *M. latifolia* extracts, including MLL. On the other hand, many flavonoid compounds from plants have been reported to inhibit HCV replication [11,20].

M. multiglandulosa is a plant that belongs to the Euphorbiaceae family. There is no report so far regarding the possible antiviral activities of *M. multiglandulosa* extracts, including MMS. However, a butanol extract of another plant in the same family, *Excoecaria agallocha*, was reported to exert potential inhibitory effects on HCV NS3/4A protease [21]. Activity-guided fractionation and structure determination revealed that four polyphenol compounds of *E. agallocha*, such as excoecariphenol D, corilagin, geraniin and chebulagic acid, inhibited HCV NS3/4A protease activities and HCV RNA replication in cultured cells harbouring an HCV RNA replicon with IC_{50} of 12.6, 13.6, 33.2 and 22.3 μM, respectively.

F. fistulosa belongs to the genus *Ficus* in the family Moraceae. Many *Ficus* species have been used in folk medicine with various pharmacological actions against convulsion, respiratory disorder, tuberculosis and other infections. Plants from genus *Ficus* are rich sources of prenylated flavonoids, isoflavonoids, lignans, terpenoids, alkaloids and coumarins. Flavonoid compounds, such as β-amyrin, alpinum isoflavone, genistein, laburnetin, luteolin and catechin, isolated from *F. chlamydocarpa* and *F. cordata* were reported to have antibacterial and antifungal activities [22]. Also, antiviral activities against HSV-1, echovirus and adenovirus were detected in extracts of *F. carica* [23] and anti-HSV-1 activities in *F. binjamina* [24]. Bioassay-guided subfractionation of a flavonoid fraction of *F. benjamina* led to identification of three flavone glycosides; quersetin 3-O-rutinoside, kaempferol 3-O-rutinoside and kaempferol 3-O-robinobioside, which showed antiviral activities against HSV-1 with IC_{50} of 1.5 ± 0.56, 3.0 ± 0.97 and 0.9 ± 0.23 μM, respectively [25]. There have been no reports on anti-HCV activities in *F. fistulosa* extracts, including FFL.

The extracts of TSL, MLL, MMS and FFL may inhibit various steps of HCV life cycle. The viral life cycle can be divided into three major steps: (i) viral attachment and entry to the target cells, (ii) synthesis and processing of the viral proteins and replication of the viral genome, and (iii) assembly and release of the viral particles [1,2]. To explore the anti-HCV mechanisms of the plant extracts, time-of-addition analysis was performed in this study. The results obtained revealed that the extracts of TSL and MLL inhibited HCV infection at both the entry and post-entry steps whereas MMS and FFL extracts principally at the entry step (Table 2). In this connection, it should be noted that, despite the fact that the extracts of TSL and MLL inhibited HCV J6/JFH1 infection at the post-entry step, neither of them inhibited HCV RNA

replication in an HCV-1b full-genomic RNA replicon system (data not shown). However, this does not necessarily rule out the possibility that these compounds may have proven efficacious if a genotype 2a replicon system had been used instead. This result rather suggests that the viral sensitivity to an antiviral plant extract(s) varies with different strains of HCV. Likewise, we observed that the sensitivity of the H77C/JFH1 strain to the FFL extract was much weaker compared to the other HCV strains (Table 3).

A flavonoid compound of green tea (*Camellia sinensis*), (−)-Epigallocatechin-3-gallate, was reported to inhibit HCV infection at the entry step with IC_{90} of 50 μM [26]. Another flavonoid from *Marrubium peregrinum L*, ladanein (BJ486K), inhibited the entry step, but not RNA replication or assembly, of HCV infection with IC_{50} of 2.5 μM [20]. On the other hand, silymarin, an extract of *Silybum marianum*, was reported to inhibit HCV entry, replication and cell-to-cell transmission with IC_{50} of 40 to 100 μM [27]. Silibinin, the major component of silymarin consisting of two flavonolignans, silibinin A and silibinin B, has currently been used to prevent reinfection of the graft after liver transplantation [28]. An increasing body of information on natural compounds possessing anti-HCV activities is summarized elsewhere [6]. As for the TSL, MLL, MMS and FFL, further analyses will be needed to determine the possible anti-HCV compounds present in their extracts. In this connection, we observed in a preliminary experiment that TSL, MLL, MMS and FFL showed anti-measles virus activities (data not shown). This result suggests that the compounds present in the extracts inhibit viral and/or cellular machineries commonly used for replication of different viruses. This should also be clarified by further mechanistic studies.

Conclusions

Ethanol extracts of *Toona sureni* leaves (TSL), *Melicope latifolia* leaves (MLL), *Melanolepis multiglandulosa* stem (MMS), and *Ficus fistulosa* leaves (FFL) inhibited the hepatitis C virus (HCV) J6/JFH1-P1 and P-47 strains with IC_{50} ranging between 2.0 and 17.1 μg/ml. All of the HCV genotypes 1a to 7a, 1b and 2b were inhibited by the plant extracts to the same extent, with the exception that the H77C/JFH1 strain of HCV genotype 1a showed significant resistance to FFL, and the J8/JFH1 (2b) and QC69/JFH1 strains (7a) to MMS to lesser extents. As for the mode of action, TSL and MLL inhibited HCV infection both at the entry and post-entry steps while MMS and FFL principally at the entry step.

Materials and methods

Cells and viruses

Huh7.5 cells and the plasmid pFL-J6/JFH1 to produce the J6/JFH1 strain of HCV genotype 2a [15] were kindly provided by Dr. C. M. Rice, The Rockefeller University, New York, NY. The plasmid for the original JFH1 strain [16] was kindly provided by Dr. T. Wakita, National Institute of Infectious Diseases, Tokyo, Japan and those for other HCV genotypes, pH77C/JFH1 (1a), pJ4/JFH1 (1b), pJ8/JFH1 (2b), pS52/JFH1 (3a), pED43/JFH1 (4a), pSA13/JFH1 (5a), pHK6a/JFH1 (6a) and pQC69/JFH1 (7a) [3], were kindly provided by Dr. J. Bukh, Copenhagen University Hospital, Hvidovre, Denmark. Huh7.5 cells were cultivated in Dulbecco's modified Eagle's medium (Wako, Osaka, Japan) supplemented with fetal bovine serum (Biowest, Nuaille, France), non-essential amino acids (Invitrogen, Carlsbad, CA), penicillin (100 IU/ml) and streptomycin (100 μg/ml) (Invitrogen). Cells were grown at 37°C in a 5% CO_2 incubator.

Collection and extraction of medicinal plants

Seventeen species of medicinal plants were collected at Cangar forest, the East Java region of Indonesia. The plants collected were verified by botanical researchers at Purwadadi Botanical Garden, Purwadadi, Indonesia. Parts of the plants were dried at room temperature and pulverized on the basis of their characteristics. They were macerated in 80% ethanol for overnight to extract constituents. After 24 hours, the extracts were filtered and the residue was soaked again in fresh solvents. The filtration process was repeated over 3 days. The filtrates were evaporated by using an evaporator at temperature not exceeding 40°C. The extracts for bioassay were dried in vacuo before being used.

Sample stock preparations

The dried ethanol extracts were weighed 10.0 mg and suspended in 100 μl of dimethyl sulfoxide (DMSO) to obtain stock solutions at a concentration of 100 mg/ml. The stock solutions were stored at −20°C until used.

Analysis of anti-HCV activities of plant extracts

Huh7.5 cells were seeded in 24-well plates (1.9×10^5 cells/well). A fixed amount of HCV was mixed with serial dilutions of medicinal plant extracts (500, 100, 50, 10 and 1 μg/ml) and inoculated to the cells. After 2 hours, the cells were washed with medium to remove the residual virus and further incubated in the medium containing the same concentrations of the plant extracts as those during virus inoculation. In some experiments, treatment with medicinal plant extracts was done only during virus inoculation or only after virus inoculation for the remaining period of the culture until virus harvest in order to assess the mode of action of the plant extracts. Culture supernatants were obtained at 1 and 2 days post-infection (dpi) and titrated for virus infectivity expressed as focus-forming units/ml, as described previously [14]. Virus and cells treated with medium

containing 0.1% DMSO served as a control. Percent inhibition of the virus infectivity by the samples was calculated by comparing to the control by using SPSS probit analysis, and IC_{50} values were determined. Percent inhibition of the compounds at the concentration of 30 μg/ml was determined also for the other genotypes of HCV.

Immunoblotting

Cells were lysed with SDS sample buffer, and equal amounts of protein were subjected to SDS-polyacrylamide gel electrophoresis and transferred onto a polyvinylidene difluoride membrane (Millipore, Bedford, MA), which was then incubated with the respective primary antibody. The primary antibodies used were mouse monoclonal antibodies against HCV NS3 and glyceraldehyde-3-phosphate dehydrogenase (GAPDH) (Millipore). Horseradish peroxidase-conjugated goat anti-mouse immunoglobulin (Invitrogen) was used to visualize the respective proteins by means of an enhanced chemiluminescence detection system (ECL; GE Healthcare, Buckinghamshire, UK).

Real-time quantitative RT-PCR

Total RNA was extracted from the cells using a ReliaPrep RNA cell miniprep system (Promega, Madison, WI) according to the manufacturer's instructions. One μg of total RNA was reverse transcribed using a GoScript Reverse Transcription system (Promega) with random primers and was subjected to quantitative real-time PCR analysis using SYBR Premix Ex Taq (TaKaRa, Kyoto, Japan) in a MicroAmp 96-well reaction plate and an ABI PRISM 7500 system (Applied Biosystems, Foster City, CA). The primers used to amplify an NS5A region of the HCV genome were 5'-AGACGTATTGAGGT CCATGC-3' (sense) and 5'-CCGCAGCGACGGTGCT GATAG-3' (antisense). As an internal control, human GAPDH gene expression levels were measured using primers 5'-GCCATCAATGACCCCTTCATT-3' (sense) and 5'-TCTCGCTCCTGGAAGATGG-3'.

WST-1 assay for cytotoxicity

WST-1 assay was performed as described previously with a slight modification [29]. In brief, Huh7.5 cells in 96-well plates were treated with serial dilutions of the medicinal plant extracts or 0.1% DMSO as a control for 48 hours. After the treatment, 10 μl of WST-1 reagent (Roche, Mannheim, Germany) was added to each well and cells were cultured for 4 hours. The WST-1 reagent is absorbed by the cells and converted to formazan by mitochondrial dehydrogenases. The amount of formazan, which correlates with the number of living cells, was determined by measuring the absorbance of each well using a microplate reader at 450 nm and 630 nm. Percent cell viability compared to the control was calculated for each dilution of the plant extracts and CC_{50} values were determined by SPSS probit analysis.

Abbreviations

CC_{50}: 50% cytotoxic concentration; DMSO: Dimethyl sulfoxide; FFL: *Ficus fistulosa* leaves; HCV: Hepatitis C virus; IC_{50}: 50% inhibitory concentration; MMS: *Melanolepis multiglandulosa* stem; MLL: *Melicope latifolia* leaves; TSL: *Toona sureni* leaves.

Competing interests

The authors declare that they have no competing interests.

Authors' contributions

TSW, AAP, EA, MA, IS, LD and CA contributed to anti-HCV bioassay work. TSW, LT, AW, AR and AF contributed to exploration and phytochemistry work. HF and NK participated in phytochemistry work. MIL, S, N, CA and HH, as principle investigators, planned and coordinated the study. TSW, LD and HH wrote the manuscript. All the authors read and approved the final manuscript.

Acknowledgements

The authors are grateful to Dr. C. M. Rice (The Rockefeller University, New York, NY) for providing Huh-7.5 cells and pFL-J6/JFH1 for the HCV genotype 2a. Thanks are also due to Dr. T. Wakita (National Institute of Infectious Diseases, Tokyo, Japan) for providing pFL-JFH1 and Dr. J. Bukh (Copenhagen University Hospital, Hvidovre, Denmark) for providing the plasmids for the other HCV genotypes; pH77C/JFH1 (1a), pJ4/JFH1 (1b), pJ8/JFH1 (2b), pS52/JFH1 (3a), pED43/JFH1 (4a), pSA13/JFH1 (5a), pHK6a/JFH1 (6a) and pQC69/JFH1 (7a). This study was supported in part by Science and Technology Research Partnerships for Sustainable Development (SATREPS) from Japan Science and Technology Agency (JST), Japan International Cooperation Agency (JICA) and the Ministry of Research and Technology (RISTEK), Republic of Indonesia. This study was also carried out as part of Japan Initiative for Global Research Network on Infectious Diseases (J-GRID), Ministry of Education, Culture, Sports, Science and Technology, Japan, and the Global Center of Excellence (G-COE) Program at Kobe University Graduate School of Medicine.

Author details

[1]Department of Pharmacognocy and Phytochemistry, Faculty of Pharmacy, Airlangga University, Surabaya, Indonesia. [2]Institute of Tropical Disease, Airlangga University, Surabaya, Indonesia. [3]Division of Microbiology, Kobe University Graduate School of Medicine, Kobe, Japan. [4]Research Center for Medicinal Plant Resources, National Institute of Biomedical Innovation, Tsukuba, Ibaraki, Japan. [5]JST/JICA SATREPS, Kobe University Graduate School of Medicine, Kobe, Japan.

Received: 1 June 2013 Accepted: 9 August 2013
Published: 13 August 2013

References

1. Moradpour D, Penin F, Rice CM: **Replication of hepatitis C virus.** *Nat Rev Microbiol* 2007, **5**:453–463.
2. Ploss A, Dubuisson J: **New advances in the molecular biology of hepatitis C virus infection: towards the identification of new treatment targets.** *Gut* 2012, **61**(Suppl 1):i25–i35.
3. Gottwein JM, Scheel TK, Jensen TB, Lademann JB, Prentoe JC, Knudsen ML, Hoegh AM, Bukh J: **Development and characterization of hepatitis C virus genotype 1–7 cell culture systems: role of CD81 and scavenger receptor class B type I and effect of antiviral drugs.** *Hepatology* 2009, **49**:364–377.
4. Arzumanyan A, Reis HM, Feitelson MA: **Pathogenic mechanisms in HBV- and HCV-associated hepatocellular carcinoma.** *Nat Rev Cancer* 2013, **13**:123–135.
5. Shepard CW, Finelli L, Alter MJ: **Global epidemiology of hepatitis C virus infection.** *Lancet Infect Dis* 2005, **5**:558–567.
6. Calland N, Dubuisson J, Rouille Y, Seron K: **Hepatitis C virus and natural compounds: a new antiviral approach?** *Virus* 2012, **4**:2197–2217.
7. Jassim SA, Naji MA: **Novel antiviral agents: a medicinal plant perspective.** *J Appl Microbiol* 2003, **95**:412–427.

8. Hussein G, Miyashiro H, Nakamura N, Hattori M, Kakiuchi N, Shimotohno K: **Inhibitory effects of sudanese medicinal plant extracts on hepatitis C virus (HCV) protease.** *Phytother Res* 2000, **14**:510–516.
9. Wu SF, Lin CK, Chuang YS, Chang FR, Tseng CK, Wu YC, Lee JC: **Anti-hepatitis C virus activity of 3-hydroxy caruilignan C from Swietenia macrophylla stems.** *J Viral Hepat* 2012, **19**:364–370.
10. Ravikumar YS, Ray U, Nandhitha M, Perween A, Raja Naika H, Khanna N, Das S: **Inhibition of hepatitis C virus replication by herbal extract: Phyllanthus amarus as potent natural source.** *Virus Res* 2011, **158**:89–97.
11. Khachatoorian R, Arumugaswami V, Raychaudhuri S, Yeh GK, Maloney EM, Wang J, Dasgupta A, French SW: **Divergent antiviral effects of bioflavonoids on the hepatitis C virus life cycle.** *Virology* 2012, **433**:346–355.
12. Bachmetov L, Gal-Tanamy M, Shapira A, Vorobeychik M, Giterman-Galam T, Sathiyamoorthy P, Golan-Goldhirsh A, Benhar I, Tur-Kaspa R, Zemel R: **Suppression of hepatitis C virus by the flavonoid quercetin is mediated by inhibition of NS3 protease activity.** *J Viral Hepat* 2012, **19**:e81–e88.
13. Nugraha AS, Keller PA: **Revealing indigenous Indonesian traditional medicine: anti-infective agents.** *Nat Prod Commun* 2011, **6**:1953–1966.
14. Bungyoku Y, Shoji I, Makine T, Adachi T, Hayashida K, Nagano-Fujii M, Ide YH, Deng L, Hotta H: **Efficient production of infectious hepatitis C virus with adaptive mutations in cultured hepatoma cells.** *J Gen Virol* 2009, **90**:1681–1691.
15. Lindenbach BD, Evans MJ, Syder AJ, Wolk B, Tellinghuisen TL, Liu CC, Maruyama T, Hynes RO, Burton DR, McKeating JA, Rice CM: **Complete replication of hepatitis C virus in cell culture.** *Science* 2005, **309**:623–626.
16. Wakita T, Pietschmann T, Kato T, Date T, Miyamoto M, Zhao Z, Murthy K, Habermann A, Krausslich HG, Mizokami M, *et al*: **Production of infectious hepatitis C virus in tissue culture from a cloned viral genome.** *Nat Med* 2005, **11**:791–796.
17. Nawawi A, Nakamura N, Hattori M, Kurokawa M, Shiraki K: **Inhibitory effects of Indonesian medicinal plants on the infection of herpes simplex virus type 1.** *Phytother Res* 1999, **13**:37–41.
18. O'Donnell F, Ramachandran VN, Smyth TJ, Smyth WF, Brooks P: **An investigation of bioactive phytochemicals in the leaves of Melicope vitiflora by electrospray ionisation ion trap mass spectrometry.** *Anal Chim Acta* 2009, **634**:115–120.
19. Higa M, Imamura M, Ogihara K, Suzuka T: **Isolation of five new flavonoids from Melicope triphylla.** *Chem Pharm Bull (Tokyo)* 2013, **61**:384–389.
20. Haid S, Novodomska A, Gentzsch J, Grethe C, Geuenich S, Bankwitz D, Chhatwal P, Jannack B, Hennebelle T, Bailleul F, *et al*: **A plant-derived flavonoid inhibits entry of all HCV genotypes into human hepatocytes.** *Gastroenterology* 2012, **14**:213–222 e215.
21. Li Y, Yu S, Liu D, Proksch P, Lin W: **Inhibitory effects of polyphenols toward HCV from the mangrove plant Excoecaria agallocha L.** *Bioorg Med Chem Lett* 2012, **22**:1099–1102.
22. Kuete V, Ngameni B, Simo CC, Tankeu RK, Ngadjui BT, Meyer JJ, Lall N, Kuiate JR: **Antimicrobial activity of the crude extracts and compounds from Ficus chlamydocarpa and Ficus cordata (Moraceae).** *J Ethnopharmacol* 2008, **120**:17–24.
23. Lazreg Aref H, Gaaliche B, Fekih A, Mars M, Aouni M, Pierre Chaumon J, Said K: **In vitro cytotoxic and antiviral activities of Ficus carica latex extracts.** *Nat Prod Res* 2011, **25**:310–319.
24. Yarmolinsky L, Zaccai M, Ben-Shabat S, Mills D, Huleihel M: **Antiviral activity of ethanol extracts of Ficus binjamina and Lilium candidum in vitro.** *N Biotechnol* 2009, **26**:307–313.
25. Yarmolinsky L, Huleihel M, Zaccai M, Ben-Shabat S: **Potent antiviral flavone glycosides from Ficus benjamina leaves.** *Fitoterapia* 2012, **83**:362–367.
26. Calland N, Albecka A, Belouzard S, Wychowski C, Duverlie G, Descamps V, Hober D, Dubuisson J, Rouille Y, Seron K: **(−)-Epigallocatechin-3-gallate is a new inhibitor of hepatitis C virus entry.** *Hepatology* 2012, **55**:720–729.
27. Wagoner J, Negash A, Kane OJ, Martinez LE, Nahmias Y, Bourne N, Owen DM, Grove J, Brimacombe C, McKeating JA, *et al*: **Multiple effects of silymarin on the hepatitis C virus lifecycle.** *Hepatology* 2010, **51**:1912–1921.
28. Barcena R, Moreno A, Rodriguez-Gandia MA, Albillos A, Arocena C, Blesa C, Garcia-Hoz F, Graus J, Nuno J, Lopez-Hervas P, *et al*: **Safety and anti-HCV effect of prolonged intravenous silibinin in HCV genotype 1 subjects in the immediate liver transplant period.** *J Hepatol* 2013, **58**:421–426.
29. Deng L, Adachi T, Kitayama K, Bungyoku Y, Kitazawa S, Ishido S, Shoji I, Hotta H: **Hepatitis C virus infection induces apoptosis through a Bax-triggered, mitochondrion-mediated, caspase 3-dependent pathway.** *J Virol* 2008, **82**:10375–10385.

doi:10.1186/1743-422X-10-259
Cite this article as: Wahyuni *et al.*: Antiviral activities of Indonesian medicinal plants in the East Java region against hepatitis C virus. *Virology Journal* 2013 **10**:259.

14-3-3 proteins sequester a pool of soluble TRIM32 ubiquitin ligase to repress autoubiquitylation and cytoplasmic body formation

Tohru Ichimura[1,2,*], Masato Taoka[2], Ikuo Shoji[3], Hiroki Kato[4], Tomonobu Sato[5], Shigetsugu Hatakeyama[5], Toshiaki Isobe[2] and Naomi Hachiya[4]

[1]Department of Applied Chemistry, National Defense Academy, Yokosuka, Kanagawa 239-8686, Japan
[2]Department of Chemistry, Tokyo Metropolitan University, Hachioji, Tokyo 192-0397, Japan
[3]Division of Microbiology, Kobe University Graduate School of Medicine, Kobe 650-0017, Japan
[4]Department of Neurophysiology, Tokyo Medical University, Shinjuku, Tokyo 160-8402, Japan
[5]Department of Biochemistry, Hokkaido University Graduate School of Medicine, Sapporo, Hokkaido 060-8638, Japan
*Author for correspondence (ichimura@nda.ac.jp)

Accepted 28 January 2013
Journal of Cell Science 126, 2014–2026

doi: 10.1242/jcs.122069

Summary

Deregulated expression of tripartite motif-containing protein 32 (TRIM32, an E3 ubiquitin-protein ligase) contributes to various diseases. Here we report, using quantitative proteomics and biochemistry, that 14-3-3 proteins bind to phosphorylated TRIM32 and prevent TRIM32 autoubiquitylation and the formation of TRIM32-containing cytoplasmic bodies, which are potential autoregulatory mechanisms that can reduce the concentration of soluble free TRIM32. The 14-3-3–TRIM32 interaction is dependent on protein-kinase-A-catalyzed phosphorylation of TRIM32 at Ser651. We found that the inhibitory effect of 14-3-3 is, in part, a consequence of disrupting the propensity of TRIM32 to undergo higher-order self-association without affecting its dimerization. Consequently, dimerized TRIM32 bound to 14-3-3 was sequestered in a distinct cytoplasmic pool away from the microtubule network, whereas a TRIM32 mutant that cannot bind 14-3-3 underwent multimerization and was unavailable to facilitate cell growth. Our results reveal a novel connection between ubiquitylation and phosphorylation pathways, which could modulate a variety of cell events by stimulating the formation of the 14-3-3–TRIM32 signaling complex.

Key words: Phosphorylation, Ubiquitylation, PKA, 14-3-3, TRIM32

Introduction

Tripartite motif-containing protein 32 (TRIM32) is a member of the expanding family of TRIM proteins that are also known as RBCC proteins as they contain a RING finger, one or two B-boxes, and a predicted coiled-coil domain (Reymond et al., 2001). The RBCC motif is usually followed by additional and variable C-terminal domains, including the SP1a and ryanodine receptor (SPRY) domain, the plant homeodomain (PHD), and the NCL-1, HT2A and LIN-41 (NHL) domain, which are specific to individual TRIMs and are thought to mediate protein–protein interactions (Reymond et al., 2001). The human genome encodes more than 70 TRIM members, and homologs have also been identified in various species. Several TRIM family members, including TRIM32, are implicated in diverse biological processes such as cell proliferation, differentiation, development, oncogenesis, apoptosis and antiviral response (Nisole et al., 2005; Hatakeyama, 2011). Despite the prevalence of TRIM genes in many species and their implication in various cell processes, whether and how these proteins, in particular TRIM32, are regulated by cellular signaling is largely unknown.

TRIM32 is an RBCC-NHL-type TRIM member originally identified as a binding partner for the activation domain of retroviral Tat (Fridell et al., 1995). TRIM32 is ubiquitously expressed in mammalian tissues, but the level varies depending on cell type and conditions (Fridell et al., 1995; Frosk et al., 2002; Horn et al., 2004; Kano et al., 2008). Abnormally high expression has been demonstrated in human skin cancer cells (Horn et al., 2004) and in the occipital lobe of Alzheimer's disease patients (Yokota et al., 2006). Moreover, *Trim32*-null mice display several myopathic and neurogenic phenotypes (Kudryashova et al., 2009); the common missense mutation D489N, which directly causes limb-girdle muscular dystrophy type 2H (LGMD2H), was recently shown to destabilize TRIM32, leading to its degradation in cells (Kudryashova et al., 2011). Like many TRIMs, TRIM32 has two potential autoregulatory properties. One is that it often self-associates and forms insoluble high-molecular-mass puncta called cytoplasmic bodies (CBs) when transiently expressed in cells (Albor et al., 2006; Locke et al., 2009). Although the role of CBs in TRIM32 functions is not fully understood, recent studies, particularly with TRIM19 and TRIM5, have suggested that CBs may function as aggresome precursors or storage compartments that maintain the proper level of soluble free TRIM proteins (Song et al., 2005; Diaz-Griffero et al., 2006) or exchange the proteins between CBs and a more diffuse cytoplasmic fraction (Campbell et al., 2007). Another property is that TRIM32 has autoubiquitylation activity in addition to conventional ubiquitin-protein ligase activity (here called transubiquitylation) (Kudryashova et al., 2005; Albor et al.,

2006). Autoubiquitylation is used by E3 ligases to regulate their own levels in cells, although it may also serve as a signal for localization and trafficking. It was recently reported that TRIM32 overexpression can promote cell proliferation, transforming activity, and cell motility and prevent apoptosis through the ubiquitin–proteasome system (Albor et al., 2006; Kano et al., 2008). It was also shown that TRIM32 overexpression can induce neuronal differentiation by activating functions of the microRNA *let7* (Schwamborn et al., 2009). Together, these findings strongly suggest that proper control of cellular TRIM32 concentration is crucial for the maintenance of normal cell growth, differentiation and function.

Although the importance of phosphorylation in substrate recognition by E3 ligases is well documented, relatively few studies have demonstrated the direct role of ligase phosphorylation in functional regulation. We and others have demonstrated that phosphorylation by protein kinase A (PKA) or SGK1 kinase negatively regulates Nedd4-2, a HECT-type E3 ubiquitin ligase, by recruiting the protein 14-3-3 (Bhalla et al., 2005; Ichimura et al., 2005; Nagaki et al., 2006). The 14-3-3 proteins constitute a diverse family of eukaryotic proteins that bind a variety of enzymes and signaling molecules in response to protein phosphorylation and modulate their activity, stability, conformation, interactions and intracellular localization. In this study we have demonstrated a wider repertoire of the 14-3-3-assited control of E3 ubiquitin ligases using mass-spectrometry-based quantification. Our results identify TRIM32, in addition to six other ubiquitin ligases including Nedd4-2, as a PKA-regulated interactor of 14-3-3 and provide a potential mechanism for the PKA/14-3-3-dependent regulation of TRIM32.

Results

Quantitative proteomic screening of 14-3-3 interactions in PKA signaling pathways in cells

To identify novel interactions of 14-3-3 in PKA signaling pathways, we employed a previously published proteomics technology combined with the tandem affinity purification tag, called MEF (myc-TEV-FLAG) (Ichimura et al., 2005; Ichimura et al., 2008). Thus, PC12Mh cells [a monoclonal PC12 cell line stably expressing the MEF-fused 14-3-3η isoform (Ichimura et al., 2005)] were labeled in medium containing [^{13}C]Lys and [^{13}C]Arg and stimulated for 20 minutes with 50 μM forskolin, a PKA activator. Lysate from stimulated cells was mixed with an equal amount of lysate from unlabeled, non-stimulated cells, and interacting partners that associated specifically with the expressed MEF-η were purified from the combined cell lysates using MEF tag-based multistep immunoaffinity purification and then identified and quantified by two-dimensional liquid chromatography–tandem mass spectrometry (Fig. 1A). We carried out this analysis five times with five independent preparations and identified 324 proteins that interact with 14-3-3, of which 200 (62%) were recovered from at least two of the five tests (supplementary material Table S1; Fig. 1B). To obtain a global view of the identified interactions, we examined the distribution of the mean log (ratio) of the response to forskolin stimulation for the 200 reproducible proteins (Fig. 1C). In contrast to many proteins that have normal and narrow range responses, several of the 200 proteins clearly showed highly variable profiles. We selected 51 proteins that displayed at least a twofold enrichment (32 proteins) or exclusion (19 proteins) in the 200-protein dataset as candidate forskolin-regulated 14-3-3 targets (Table 1). Interestingly, although 33 of the 51 proteins (65%) have been reported to bind 14-3-3s (see Table 1), the involvement of PKA in their association has been limited to only five interactors: CaMKKα, Nedd4-2, PDE3A, TH and TORC2.

To directly assess the contribution of PKA to the observed interactions, we performed a co-transfection assay using the catalytic subunit of PKA (cPKA). We chose 11 proteins based on three criteria: known targets for 14-3-3 in PKA signaling (CaMKKα, Nedd4-2, TH, TORC2), known targets for 14-3-3 but unknown for their interactions in PKA signaling (TRIM32, TPD52L1, WDR20, AKT1S1, TFEB), and those implicated in neither 14-3-3 binding nor PKA signaling (SMURF1, RNF20). Intriguingly, all of the associations to be tested, except for that of TFEB, were successfully reconstituted by coexpression of cPKA even in the absence of forskolin in HEK293 cells (supplementary material Fig. S1A). For TFEB, association was reconstituted in PC12 cells but not in HEK293, probably reflecting cell-type specificity for this interaction (supplementary material Fig. S1B, right panel). These results demonstrated the utility of our proteomic procedure to identify novel interactions and strongly suggested that most, if not all, of the interactions selected in this screen were located downstream of PKA.

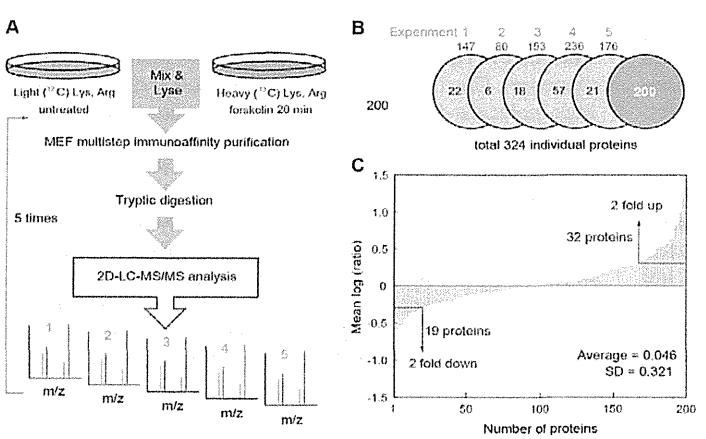

Fig. 1. Quantitative 14-3-3 interactome analysis in PKA signaling pathways. (**A**) Strategy for identifying and quantifying 14-3-3 interactions in PKA signaling pathways. 2D, two-dimensional; LC, liquid chromatography; MS/MS, tandem mass spectrometry. (**B**) Characterization of 14-3-3 interactors identified from five analyses. The figure shows the number of proteins consistently identified in at least two analyses (200 proteins total) and the number of uniquely identified proteins in each analysis. (**C**) Relative interaction change of the reproducibly identified proteins plotted logarithmically. The cutoff points (±2-fold change) are indicated by arrows.

Table 1. Summary of forskolin-responsive 14-3-3 binding targets identified by LC-MS/MS

Human homolog	Protein description	Ratio[a]	Binding	Human homolog	Protein description	Ratio[a]	Binding
Upregulated proteins				Downregulated proteins			
CAMKK1	Calcium/calmodulin-dependent protein kinase kinase 1, alpha	15.83	Yes	UPF1	Regulator of nonsense transcripts 1	0.50	Yes
SPECCIL	Cytospin A	15.01	No	WASF2	Wiskott-Aldrich syndrome protein family member 2	0.50	Yes
PDE3A	Phosphodiesterase 3A	10.37	Yes	PLEKHA7	Pleckstrin homology domain containing, family A member 7	0.47	Yes
TH	Tyrosine hydroxylase	9.78	Yes	TFEB	transcription factor EB	0.45	Yes
TPD52L2	Tumor protein D52-like 2	7.21	Yes	SIPA1L3	Signal-induced proliferation-associated 1 like 3	0.44	Yes
MAST1	Microtubule associated serine/threonine kinase 1	6.80	No	ARHGAP23	PREDICTED: Rho GTPase activating protein 23	0.44	Yes
PNPLA7	Patatin-like phospholipase domain containing 7	6.78	No	LOC652055	Similar to slit homolog 1	0.43	No
MFF	Mitochondrial fission factor	4.48	Yes	SPEG	Aortic preferentially expressed gene 1	0.43	Yes
CAMSAP2	Calmodulin regulated spectrin-associated protein family, member 2	4.34	No	MLLT4	Myeloid/lymphoid or mixed-lineage leukemia; translocated to, 4	0.41	Yes
TPD52	Tumor protein D52	4.32	Yes	BSN	Bassoon (presynaptic cytomatrix protein)	0.37	No
WDR20	WD repeat domain 20	4.31	Yes	KAB	KARP-1 binding protein 1	0.37	Yes
TPD52L1	Tumor protein D52-like 1	3.85	Yes	TBC1D4	Similar to TBC1 domain family member 4	0.36	Yes
GIGYF1	GRB10 interacting GYF protein 1	3.74	Yes	KIAA1598	shootin-1	0.30	No
EPB41L3	Erythrocyte membrane protein band 4.1-like 3	3.63	Yes	HECTD1	E3 ubiquitin-protein ligase HECTD1	0.29	Yes
SMURF1	E3 ubiquitin protein ligase SMURF1	3.47	No	CRTC2	CREB regulated transcription coactivator 2 (TORC2)	0.28	Yes
ZNRF2	E3 ubiquitin-protein ligase ZNRF2	3.37	Yes	COBLL1	Cordon-bleu protein-like 1	0.27	No
RAE1	RNA export 1 homolog (S. pombe)	3.36	Yes	HDAC4	Histone deacetylase 4	0.25	Yes
FAM83E	PREDICTED: hypothetical protein	3.34	No	AKT1S1	AKT1 substrate 1 (proline-rich)	0.18	Yes
PLEKHA6	Pleckstrin homology domain containing, family A member 6	3.26	No	BLM	Bloom syndrome, RecQ helicase-like	0.12	No
CDK18	Cyclin-dependent kinase 18	3.16	Yes				
MYCBP2	E3 ubiquitin-protein ligase MYCBP2	2.80	Yes				
FLJ22471	PREDICTED: similar to DNA segment, Chr 5	2.66	No				
NEDD4L	E3 ubiquitin-protein ligase Need4-2	2.59	Yes				
RNF20	E3 ubiquitin-protein ligase RNF20	2.58	No				
RGNEF	Rho-guanine nucleotide exchange factor	2.54	No				
CASKIN1	CASK interacting protein 1	2.39	No				
MYCBP	Similar to c-myc promoter binding protein	2.29	Yes				
KCNC1	Potassium voltage-gated channel, Shaw-related subfamily, member 1	2.23	No				
TRIM32	E3 ubiquitin-protein ligase TRIM32	2.21	Yes				
KIAA0226	PREDICTED: similar to mKIAA0226 protein isoform 2	2.15	No				
FAM82A2	Regulator of microtubule dynamics protein 3	2.11	Yes				
WNK1	Serine/threonine-protein kinase WNK1	2.04	Yes				

[a]Average ratio of fold change in 14-3-3 binding with forskolin stimulation compared to basal.

Confirmation of TRIM32 as a 14-3-3 binding partner

TRIM32 was identified in the screen together with six other ubiquitin E3 ligases including Nedd4-2 (Fig. 2A). Because TRIM32, like Nedd4-2, is implicated in several inherited diseases, we selected this interaction for further analysis. We initially examined the interaction in a pull-down assay using bacterially expressed and purified 14-3-3η and GST-fused TRIM32. 14-3-3η bound to the GST–TRIM32 under conditions in which it was phosphorylated by PKA (Fig. 2B, lane 4); no complex was detected with the GST moiety alone (lanes 1 and 2) or with GST–TRIM32 in the absence of PKA (lane 3), suggesting that 14-3-3 binds directly to TRIM32 when phosphorylated by PKA. We next assessed the interaction in a co-precipitation assay using all seven mammalian 14-3-3 isoforms (η, β, γ, ε, ζ, θ, σ) tagged with myc. The interaction of all these 14-3-3 isoforms with FLAG–TRIM32 were stimulated by coexpression of cPKA in HEK293 cells (Fig. 2C), a cell line widely used in the study of TRIM32 interaction and localization (Kano et al., 2008; Locke et al., 2009; Ryu et al., 2011). Phosphate incorporation into TRIM32 under these conditions was confirmed using phospho-PKA substrate antibodies (Fig. 2C, bottom panel). Thus, TRIM32 is capable of interacting with many 14-3-3 isoforms when co-expressed in HEK293 cells. We then investigated the interaction between endogenous 14-3-3s and TRIM32. Endogenous 14-3-3s were immunoprecipitated from naive PC12 cells with PAN-14-3-3 antibodies, and the immunocomplexes were analyzed by western blotting with a TRIM32-specific antibody. TRIM32 was readily detected in the

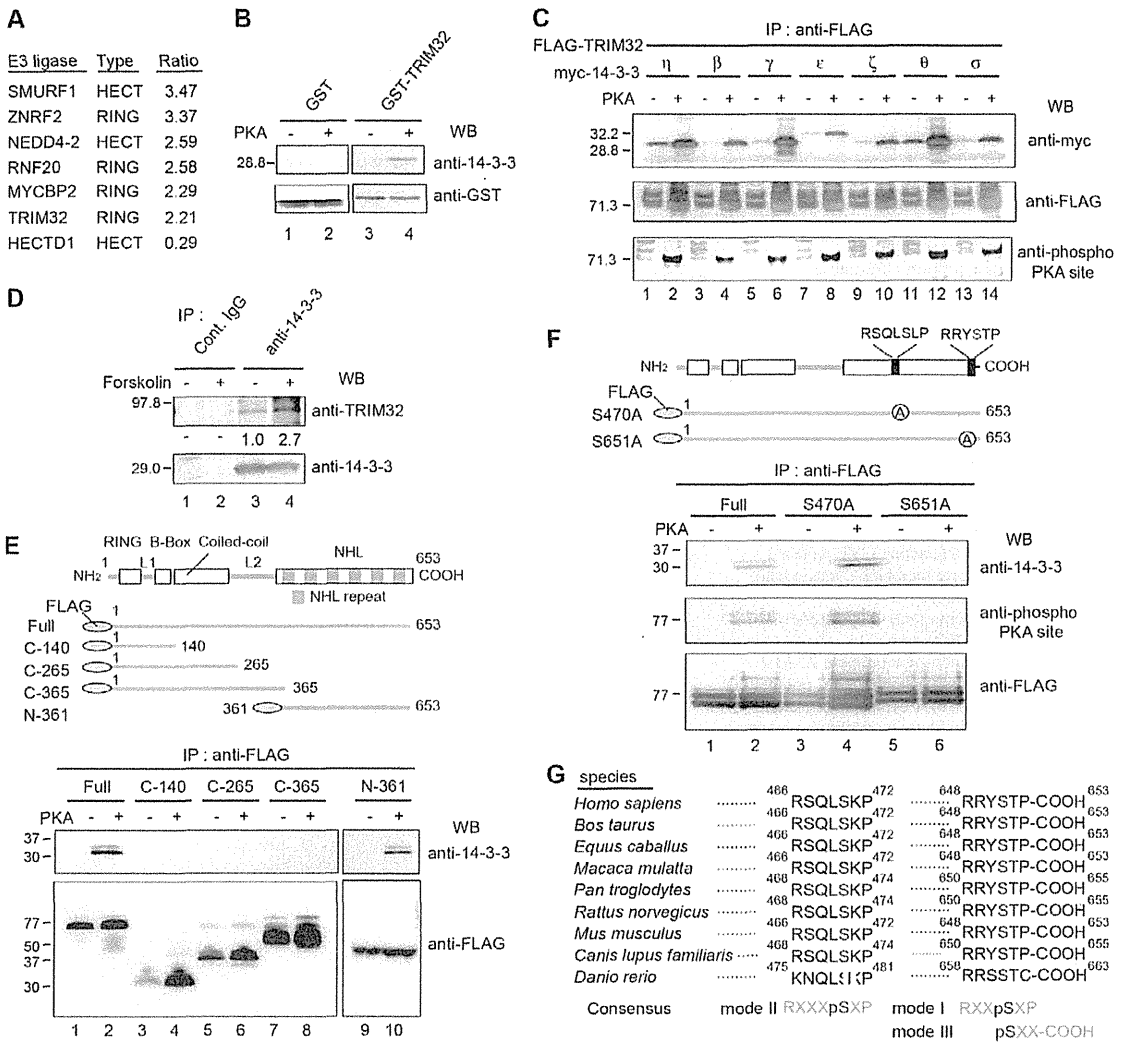

Fig. 2. Identification of TRIM32 as a PKA-regulated 14-3-3 interacting partner. (**A**) E3 ubiquitin-protein ligases identified as forskolin-responsive 14-3-3-binding partners. (**B**) *In vitro* association of 14-3-3 with phosphorylated TRIM32 as assessed by western blotting (WB). Purified GST–TRIM32 or GST alone (~0.5 μg each) was incubated with 14-3-3η (1 μg) in the absence or presence of PKA, pulled down with glutathione–Sepharose, and the precipitates were analyzed by WB with anti-PAN 14-3-3 (upper panel) and anti-GST (lower panel). (**C**) PKA-induced interaction of TRIM32 and mammalian 14-3-3 isoforms in HEK293 cells. FLAG–TRIM32 (5 μg), and myc-14-3-3η, β, γ, ε, ζ, 0 or σ (5 μg) plasmids were transfected together with or without cPKA (5 μg) into HEK293 cells at the indicated combinations. After 24 hours, the expressed FLAG–TRIM32 was immunoprecipitated (IP) with anti-FLAG–Sepharose beads, and the precipitates were analyzed by WB with monoclonal anti-myc (upper panel) and monoclonal anti-FLAG (middle panel). The middle blot was also stripped and analyzed with anti-phospho-PKA substrate (bottom panel). Molecular size markers, in kDa, are indicated at the left. (**D**) Association of endogenous 14-3-3 and TRIM32 in PC12 cells. Cells were maintained as described previously (Nagaki et al., 2006), incubated in serum-free medium for 16 hours, and then stimulated for 20 minutes with 50 μM forskolin as indicated. After IP with anti-PAN 14-3-3 (2 μg, lanes 3 and 4) or preimmune IgG (2 μg, lanes 1 and 2), the immunocomplexes were analyzed by WB with anti-TRIM32 (upper panel) or anti-PAN14-3-3 (lower panel). The intensity of each TRIM32 band shown in the upper panel (lanes 3 and 4) was also quantified by densitometry and expressed as fold change of the level in non-stimulated cells. (**E**) Analysis of the TRIM32 domain responsible for binding 14-3-3. HEK293 cells were transfected with the indicated TRIM32 constructs and cPKA (5 μg each), and the expressed TRIM32 and its truncation mutants were immunoprecipitated with anti-FLAG. The immunoprecipitates were then analyzed by WB with anti-PAN-14-3-3 and monoclonal anti-FLAG. (**F**) Effect of the TRIM32 S470A or S651A mutation on 14-3-3 binding. The experiment was conducted as in E, except that S470A and S651A point mutants of FLAG–TRIM32 (5 μg each) were used instead of the truncation mutants. The bottom blot was also stripped and reprobed with anti-phospho-PKA substrate to monitor phosphorylation (middle panel). (**G**) Conserved sequence motifs for 14-3-3 binding located in the NHL domains of known TRIM32s.

14-3-3 immunoprecipitate but not the control immunoprecipitate (Fig. 2D, lane 3). Of note, forskolin stimulation increased the TRIM32 abundance in the precipitate (lane 4), consistent with our mass spectrometry data. These results suggested that endogenous TRIM32 resides in a complex with 14-3-3s upon PKA activation. Further evidence that TRIM32 is a 14-3-3-interacting partner was obtained with a colocalization assay using FLAG–TRIM32 and myc–14-3-3η together with cPKA. The

immunostaining patterns of FLAG–TRIM32 and myc–14-3-3η were generally similar, confirming that the two proteins indeed colocalize in cells (see Fig. 3B, left panels).

14-3-3 binds TRIM32 via mode III

TRIM32 contains the tripartite RBCC domain (Reymond et al., 2001). In contrast, its C-terminus carries the unique NHL domain that includes six repeats of the 40-residue segment called the NHL repeat (Fig. 2E, upper panel). To further characterize the association of TRIM32 with 14-3-3, we generated four FLAG-tagged TRIM32 deletions (C-140, C-265, C-365, N-361; Fig. 2E), each of which was truncated either in the N- or C-terminal domain. Subsequent immunoprecipitation from HEK293 cells revealed specific co-precipitation of endogenous 14-3-3s with the expressed full-length TRIM32 as well as the N-361 fragment only in the presence of cPKA, but not with C-140, C-265 and C-365 (Fig. 2E, lower panels, lanes 2 and 10). These results suggested that the C-terminal NHL domain is necessary and sufficient for the observed 14-3-3 binding.

14-3-3 proteins recognize a phosphorylated serine or threonine residue in the consensus sequence motifs Rxx[S/T(*P*)]xP (mode I), Rxxx[S/T(*P*)]xP (mode II), or [S/T(*P*)]xx-COOH (mode III), where S/T(*P*) is phospho-Ser/Thr and x is any amino acid. Analysis of the amino acid sequence of human TRIM32 revealed that such sequence motifs indeed occur within the NHL domain encompassing Ser470 and Ser651 (Fig. 2F,G); importantly, these motifs are highly conserved in TRIM32 homologs from various organisms, although *Danio rerio* TRIM32 contains only the mode III sequence (Fig. 2G). We thus prepared two point mutants of TRIM32 that replaced either Ser residue with Ala (S470A and S651A) and tested these mutants for 14-3-3 binding in an assay similar to that described above. As shown in Fig. 2F, the interaction with endogenous 14-3-3s was completely disrupted by the S651A mutant (lower top panel, lane 6), whereas the S470A mutant had no effect (lane 4). Interestingly, S651A also caused a complete loss of binding of the PKA substrate antibody (lower middle panel, lane 6), suggesting that the antibody preferentially recognizes this site. Thus, 14-3-3 specifically interacts with TRIM32 when the ligase is phosphorylated by PKA at Ser651 within its NHL domain. The TRIM32 sequence also contains a proline two residues downstream of S(*P*)651 (Pro653), a residue that fits the consensus mode I 14-3-3 binding site (Fig. 2F,G). We found, however, that this Pro residue was not necessary for interaction with 14-3-3 because the mutant P653A could still bind 14-3-3s in a cPKA-dependent manner in an immunoprecipitation assay. Thus, 14-3-3 probably binds TRIM32 via mode III rather than mode I, which does not require Pro in that position (Ganguly et al., 2005; Coblitz et al., 2006).

14-3-3 binding affects the formation of TRIM32-containing CBs

Like many other TRIM32 constructs (Albor et al., 2006; Locke et al., 2009; Ryu et al., 2011), the FLAG-tagged TRIM32 we generated spontaneously formed CBs when transiently expressed in cultured cells (Fig. 3A, left panel). Fluorescence microscopy and electron microscopy revealed that these CBs vary in size and shape, but are approximately spherical and hollow (Fig. 3A, middle right panels), reminiscent of TRIM5α-containing CBs (Campbell et al., 2007). To investigate the functional significance of 14-3-3–TRIM32 complex formation, we monitored the effect of 14-3-3 binding on the formation of TRIM32 CBs. Coexpression of myc-14-3-3η and cPKA induced a dramatic shift of TRIM32 (but not S651A) localization from CBs to a more diffuse cytoplasmic fraction (Fig. 3B). This altered TRIM32 distribution appeared relevant because coexpression of AGO1 and Abi2, two other proteins that bind TRIM32 through its NHL domain (Kano et al., 2008; Schwamborn et al., 2009), did not cause such a change (supplementary material Fig. S2). To better dissect the role for 14-3-3 in this process, 14-3-3η was also expressed before or after transfection with TRIM32 and cPKA, and the influence of this 14-3-3 on CB formation was assessed. This experiment indicated that pre-expression of 14-3-3η caused TRIM32 redistribution similar to that observed upon coexpression of 14-3-3η, whereas post-expression with 14-3-3η did not (Fig. 3C). Moreover, post-expressed 14-3-3η did not colocalize with the pre-existing TRIM32 CBs (Fig. 3C, right panels), suggesting that the CBs, once formed, may be refractory to the accessibility of 14-3-3. These observations suggested that 14-3-3 plays a role at the initial step of CB formation through association with phosphorylated TRIM32.

Time-lapse microscopy was then performed with a fusion protein tethering cyan fluorescent protein (CFP) to TRIM32 to demonstrate the observed role for 14-3-3 in living cells. CFP–TRIM32 was initially detected within 4 hours after transfection. In these cells, small CBs formed along with faint CFP signals, and the smaller CBs coalesced to form larger CBs (Fig. 3D, top two panels). Importantly, when 14-3-3η and cPKA were co-transfected, CFP–TRIM32 was also observed to be diffuse throughout the cytoplasm with no visible CBs (Fig. 3D, middle two panels), consistent with the immunofluorescence data. CBs containing other TRIMs, e.g. TRIM19 or TRIM5α, are transported along microtubules to form larger CBs (Campbell et al., 2007). Consistent with this, we found that addition of nocodazole, a microtubule destabilizing agent, prevented the formation of larger TRIM32 CBs (Fig. 3D, bottom two panels). To further characterize the contribution of 14-3-3 to CB formation, we analyzed the association of TRIM32 with microtubules. As expected, TRIM32-bound 14-3-3η was distributed throughout the cytoplasm away from the microtubule network, whereas TRIM32 expressed without 14-3-3η was confined to CBs located along microtubules (supplementary material Fig. S3, compare top and middle panels). Because association with microtubules was seen with the S651A mutant even in the presence of 14-3-3η and cPKA (bottom panels), it is probable that our results with wild-type TRIM32 were not due to a general defect in microtubule integrity. Collectively, these results suggested that TRIM32 is specifically sequestered into a separate cytoplasmic pool in a complex with 14-3-3 prior to the incorporation into CBs. Similar results were obtained with all seven mammalian 14-3-3 isoforms (supplementary material Fig. S4), in line with the fact that these isoforms also bound TRIM32 in a cPKA-dependent manner (Fig. 2C).

14-3-3 binding prevents both TRIM32 autoubiquitylation and TRIM32 transubiquitylation

We and others have previously shown that 14-3-3 forms a stable complex with Nedd4-2 phosphorylated by SGK1 or PKA to maintain the phosphorylated ligase in an enzymatically inactive form (Bhalla et al., 2005; Ichimura et al., 2005). To examine whether 14-3-3 binding similarly affects TRIM32 activity, we

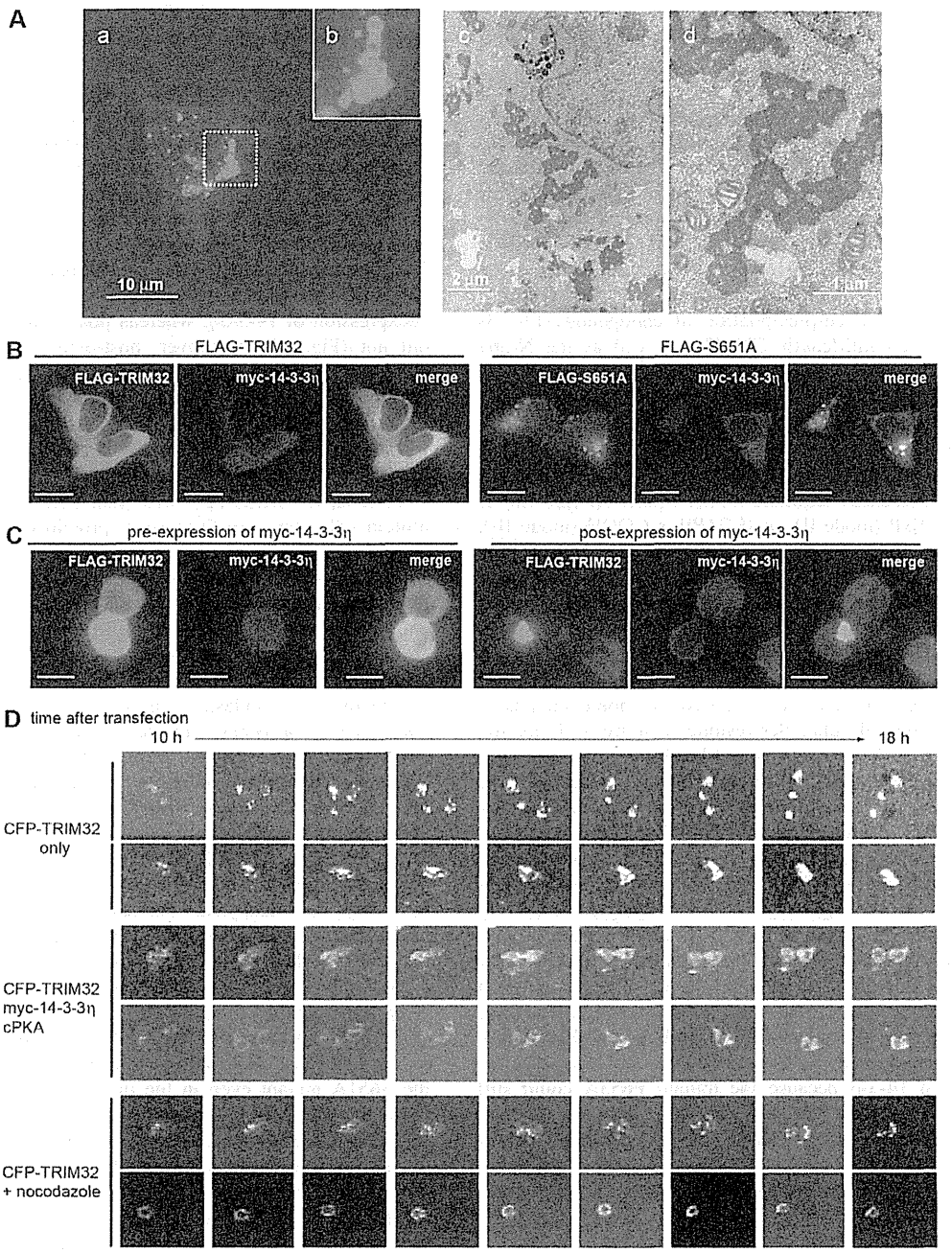

Fig. 3. 14-3-3 prevents the formation of TRIM32-containing CBs. (**A**) Immunofluorescence and electron microscopy images of TRIM32 CBs in HEK293 cells. HEK293 cells were transiently transfected with FLAG–TRIM32, and TRIM32 localization was analyzed by immunofluorescence (a,b) and electron microscopy (c,d). (**B**) Immunofluorescence double labeling of TRIM32 and its S651A mutant (both green) and 14-3-3η (red). Myc–14-3-3η, cPKA and FLAG–TRIM32 (left panels) or the S651A mutant (right panels) were transfected into HEK293 cells. After 24 hours, cells were stained with polyclonal rabbit anti-FLAG (green) and monoclonal mouse anti-myc (red). (**C**) Effect of myc-14-3-3η pre-expression and post-expression on subcellular distribution of TRIM32. The experiments were conducted as in B, except that myc-14-3-3η was expressed 24 hours before (left panels) or after (right panel) transfection with FLAG–TRIM32 and cPKA. (**D**) Time-lapse imaging with HEK293 cells expressing CFP–TRIM32 (top two panels), CFP–TRIM32, cPKA and myc-14-3-3η (middle two panels), or CFP–TRIM32 in the presence of 10 μg/ml nocodazole (bottom two panels). Cells were imaged at 1-hour intervals. Nocodazole was added 6 hours before imaging. Representative images of cells from three independent experiments are shown.

performed an in-cell ubiquitylation assay involving hemagglutinin (HA)-tagged ubiquitin (Ichimura et al., 2005) (see also Materials and Methods). Consistent with previous findings (Albor et al., 2006; Locke et al., 2009; Ryu et al., 2011), the expressed FLAG–TRIM32 was biologically active and was heavily autoubiquitylated in the cells, as demonstrated by a smear of high-molecular-mass species of HA–ubiquitin (Fig. 4A, lanes 2 and 8). We found, however, that the intensity of autoubiquitylated FLAG–TRIM32 decreased significantly in the presence of 14-3-3η and cPKA but not cPKA alone (lanes 4 and 10, compare with lanes 3 and 9). Two point mutants were used to assess the specificity of this finding; one was the V180D point mutant of 14-3-3η, which specifically disrupts the interaction of 14-3-3η with a variety of targets including Nedd4-2 (Ichimura et al., 2005), and the other was the TRIM32 S651A mutant that was deficient in 14-3-3 binding. Little reduction of TRIM32 autoubiquitylation was detected in these controls (Fig. 4A lanes 5–6, 11–12), indicating that 14-3-3 binding decreased TRIM32 autoubiquitylation. These results suggested that 14-3-3–TRIM32 complex formation suppresses TRIM32 autoubiquitylation in cells. Similar suppression was observed with all seven 14-3-3 isoforms (Fig. 4B, lanes 2–8), consistent with results from the CB formation assay (supplementary material Fig. S4).

We next tested whether 14-3-3 could also affect TRIM32-mediated transubiquitylation. To this end, we used a FLAG–Abi2 protein [a known *in vivo* substrate of TRIM32 (Kano et al., 2008)] as a model and determined its level of ubiquitylation using wild-type (non-tagged) TRIM32. TRIM32-catalyzed ubiquitylation of Abi2 decreased to almost the basal level upon coexpression of 14-3-3η and cPKA (Fig. 4C, lane 4, compare with lanes 2–3) but not with control constructs (lanes 5–6). Notably, 14-3-3 (σ isoform) is a substrate for Efp (TRIM25) (Urano et al., 2002). We thus tested whether FLAG–14-3-3η was ubiquitylated and found that this isoform was not ubiquitylated by TRIM32 under phosphorylating or nonphosphorylating conditions despite strong ubiquitylation of FLAG–Abi2 that was used as a positive control (Fig. 4D, upper panel, lanes 3–5, compare with lane 2). Indeed, coexpression of TRIM32 did not decrease the steady-state levels of exogenous FLAG–14-3-3η as well as endogenous 14-3-3 proteins, unlike the FLAG–Abi2 protein (Fig. 4D, lower panels). We confirmed this observation with FLAG–14-3-3η as well as FLAG–14-3-3σ after total HA-ubiquitylated proteins were first separated by anti-HA–Sepharose and analyzed by western blotting with anti-FLAG (Fig. 4E). Thus, the observed 14-3-3-mediated inhibition of autoubiquitylation and transubiquitylation of TRIM32 reflects a specific effect of 14-3-3 binding to phosphorylated TRIM32 rather than a more general effect such as enzyme–substrate competition.

14-3-3 blocks TRIM32 higher-order self-association but not homodimerization

To understand the molecular mechanism by which 14-3-3 represses both CB formation and E3 ubiquitin ligase activity, we investigated the effect of 14-3-3 binding on TRIM32 self-association. Two discrete modes for self-association have been described for TRIM proteins; low-order (dimerization) and high-order self-association, and dimerization is a prerequisite to efficient higher-order oligomerization (Ganser-Pornillos et al., 2011; Li et al., 2011) (see Fig. 5A). It also has been reported that higher-order interaction is implicated in the formation of TRIM-containing CBs (Ganser-Pornillos et al., 2011) and the expression of enhanced RING E3 activities (Kentsis et al., 2002; Pertel et al., 2011). We used sucrose-density-gradient centrifugation to directly compare the in-cell formed self-association complexes of TRIM32 and its S651A mutant bound or not bound with 14-3-3η. As shown in Fig. 5B, the wild-type (non-tagged) TRIM32 complexes were detected predominantly in fraction 1 as well as at the bottom of the tube that consisted of high-molecular-mass complexes (S value >16S; top panel). A similar but more sedimenting profile was obtained with the S651A mutant in the same assay (Fig. 5B, second panel). When 14-3-3η and cPKA were coexpressed in cells, however, the wild-type TRIM32 complexes, but not those containing S651A, were almost completely recovered in the lower-density fractions (~fraction 5; S value ~8S, third panel, compare with the bottom fourth panel). These results suggested that 14-3-3–TRIM32 complex formation disrupts TRIM32 higher-order self-association in cells.

We next examined whether 14-3-3 binding affects TRIM32 homodimerization. We used a detergent-solubilized cell extract as a potential source for TRIM homodimers, which is widely used for characterization of many TRIMs including TRIM32 (Locke et al., 2009). HEK293 cell extracts containing FLAG-tagged TRIM32 and the same construct tagged with myc were prepared with Triton X-100, and the resulting extract was subjected to co-immunoprecipitation to detect the TRIM32 homodimer. As can be seen in Fig. 5C (top panel, lane 2), the antibody to FLAG effectively precipitated myc–TRIM32 with FLAG–TRIM32, confirming that these tagged TRIM32s could indeed form dimers. Importantly, when the same co-immunoprecipitation was performed with extracts containing coexpressed myc-14-3-3η and cPKA, almost equal amounts of myc–TRIM32 were recovered in the FLAG–TRIM32 immunocomplex even though the expressed 14-3-3η formed a complex with FLAG–TRIM32 (Fig. 5C, top panel, lane 3). Furthermore, when the co-immunoprecipitation was carried out with myc–S651A and FLAG–S651A, a comparable amount of myc–S651A also co-precipitated with FLAG–S651A in the presence of myc-14-3-3η and cPKA (lane 4). Thus, 14-3-3 binding does not affect TRIM32 homodimerization. These results suggested that 14-3-3 binding specifically disrupts TRIM32 higher-order multimerization without affecting homodimerization. Given that higher-order self-association appears to be important for both the formation of TRIM-containing CBs and ubiquitin ligase activity (Kentsis et al., 2002; Ganser-Pornillos et al., 2011; Li et al., 2011), this may explain how a single protein interaction has so many effects.

14-3-3 modulates the level of soluble TRIM32 and its ability to accelerate growth of NIH3T3 cells

Although many TRIM proteins exist in the cytoplasm in both soluble and insoluble states, the soluble (most probably monomers and dimers) rather than insoluble forms (higher-order oligomers or CBs; see Fig. 5A) may constitute the active protein fraction (Song et al., 2005). Because our data indicated that 14-3-3 prevents both TRIM32 autoubiquitylation and the formation of TRIM32-containing CBs – potential autoregulatory mechanisms that reduce the level of soluble TRIM32 – we assumed that 14-3-3 might also modulate cellular levels of soluble TRIM32. Thus, HEK293 cell lysates containing TRIM32 together with increasing amounts of 14-3-3η and cPKA were separated into soluble and insoluble fractions by centrifugation and analyzed by western blotting. Indeed, increased 14-3-3 expression promoted an elevated level of TRIM32 in the soluble

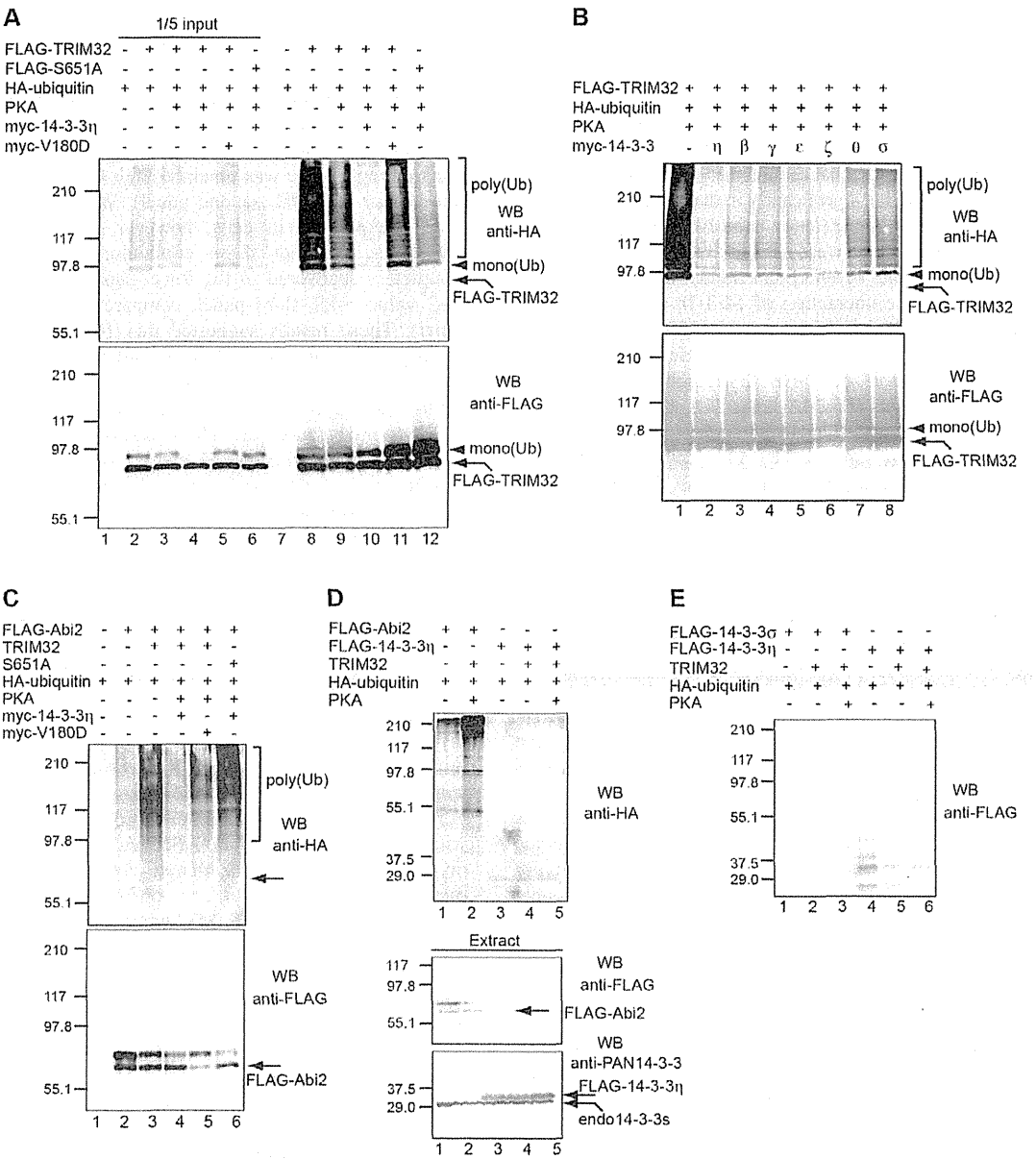

Fig. 4. 14-3-3 binding inhibits TRIM32 autoubiquitylation and TRIM32 transubiquitylation. (**A–C**) HEK293 cells transiently co-transfected with the indicated plasmids (5 μg each) were lysed with 1% SDS, and the expressed FLAG–TRIM32 (A,B) or FLAG–Abi2 (C) was immunoprecipitated with anti-FLAG. The precipitated proteins were analyzed by 7.5% SDS-PAGE followed by western blotting (WB) with monoclonal anti-FLAG to detect the precipitated TRIM32 and Abi2 (lower panels) or with monoclonal anti-HA (upper panels) to detect their ubiquitylated forms. Ubiquitylated species are indicated with bars (polyubiquitylated forms) and arrowheads (monoubiquitylated form). The arrows indicate FLAG–TRIM32 (A,B) and FLAG–Abi2 (C). Similar results were obtained for at least three independent experiments. (**D**,**E**) HEK293 cells transiently co-transfected with the indicated constructs (5 μg each) were lysed with 1% Triton X-100, and lysates were subjected to immunoprecipitation with anti-FLAG (**D**) or anti-HA (**E**) followed by 10% SDS-PAGE. Ubiquitylation of FLAG–14-3-3 was then analyzed by WB with monoclonal anti-HA (D) or anti-FLAG (E). Cell lysates (10 μg of protein each) treated as in D were also analyzed by WB to determine protein levels (lower panels). Similar results were obtained for at least three independent experiments.

fraction with a concomitant decrease in TRIM32 in the insoluble fraction (Fig. 6A). This elevation was not detected when we used cPKA or 14-3-3η alone (Fig. 6B, lanes 1–3 and 1′–3′, compare with lanes 4 and 4′) or when we transfected the V180D 14-3-3η mutant or S651A TRIM32 mutant instead of their respective wild-type constructs (Fig. 6B, lanes 5 and 6, 5′ and 6′), consistent with the data from autoubiquitylation and CB formation assays (Fig. 3B; Fig. 4A,C). The finding was supported by time-course experiments with the protein synthesis inhibitor cycloheximide (Fig. 6C). About half of the

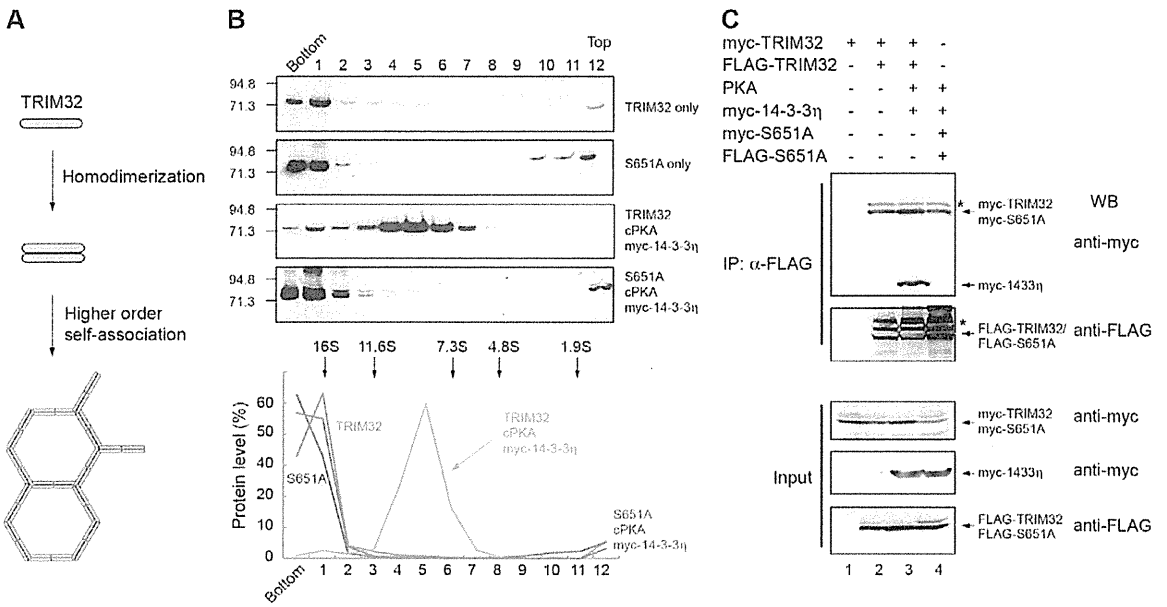

Fig. 5. 14-3-3–TRIM32 complex formation prevents TRIM32 higher-order self-association but not homodimerization. (**A**) A model of intermolecular interactions of TRIM proteins. The model is based on the proposal by Ganser-Pornillos et al. (Ganser-Pornillos et al., 2011). (**B**) HEK293 cells transiently co-transfected with the indicated constructs (5 μg each) were homogenized in PBS (pH 7.4) and subjected to sucrose density-gradient centrifugation (5–20%, 100,000 *g*, 18 hours), fractionated from the bottom, and analyzed by SDS-PAGE followed by western blotting (WB) with anti-TRIM32. The intensities of gel bands were plotted as a percentage of the total amount of protein in each experiment. Marker proteins included *Escherichia coli* galactosidase (16S), bovine catalase (11.6S), yeast alcohol dehydrogenase (7.3S), BSA (4.8S), and egg white lysozyme (1.9S). (**C**) HEK293 cells transiently transfected with the indicated plasmids (5 μg each) were lysed with 1% Triton X-100 and subjected to precipitation with anti-FLAG after normalizing levels of expressed TRIM32 proteins for each immunoprecipitation (IP) experiment. The amounts of myc- and FLAG-tagged proteins in the immunoprecipitates (upper panels) and lysates (lower panels) after normalizing the expressed protein amounts were analyzed by WB with the indicated antibodies. The asterisk denotes monoubiquitylated TRIM32/S651A.

TRIM32 expressed alone in the cells disappeared from the soluble fraction within 10–12 hours of chase, whereas in cells co-transfected with 14-3-3η and cPKA, a slower decrease in the level of soluble TRIM32, but not the S651A mutant, was detected, with a half-life of >48 hours. Notably, >60% of TRIM32 was retained in the soluble pool even after a 48-hour chase. These results suggested that the observed increase in soluble TRIM32 concentration was due to alterations in the relative half-life of the protein owing to interaction with 14-3-3.

To examine the potential biological relevance of the 14-3-3–TRIM32 interaction, we produced stable NIH3T3 cell lines that expressed FLAG–TRIM32 (WT), FLAG–S651A mutant (S651A) or an empty vector (Mock) using retroviral infection, and counted cell numbers at various time points (Fig. 6D). It is reported that NIH3T3 cells express TRIM32 naturally (Kano et al., 2008), in addition to PKA and 14-3-3. In agreement with previous data (Kano et al., 2008), the growth rate of NIH3T3 cells increased significantly upon expression of TRIM32 (WT) as compared with Mock. We observed, however, that S651A did not show any stimulatory effect on NIH3T3 cell growth under parallel conditions (growth rate similar to that of Mock). Thus, the S651A mutant, which has E3 ubiquitin-protein ligase activity (Fig. 4A, lanes 6 and 12; Fig. 4C, lane 6) yet cannot bind 14-3-3 (Fig. 2F, lane 6), could not elicit the intrinsic cell growth activity. We concluded that PKA-mediated Ser651 phosphorylation and 14-3-3 binding are important factors for regulating TRIM32.

14-3-3 and TRIM32 co-precipitate from normal tissues

The interaction data described above were obtained with cultured cells or recombinant proteins. To validate the physiological importance of the interaction of 14-3-3 with TRIM32, we tested whether endogenous TRIM32 is associated with native 14-3-3 immunopurified from mouse skeletal muscle and brain (Fig. 6E). TRIM32 was clearly co-immunoprecipitated with 14-3-3 from both these tissue homogenates but not with control IgG (lanes 2 and 5, compare with lanes 1 and 4). Importantly, this association was stimulated by addition of cAMP, ATP and magnesium chloride to the homogenates, indicating that PKA-dependent phosphorylation is involved in mediating the complex formation (lanes 3 and 6). These results suggest that a 14-3-3:phosphoTRIM32 complex exists even in normal tissues, which support the notion that this association is physiologically significant in cells.

Discussion

In the present study we show the bidirectional, coordinated response of the 14-3-3 interactome in PKA signaling pathways and identify 51 binding targets of 14-3-3η whose interactions were significantly altered upon PKA activation (Table 1). For 46 of these 51 proteins, the interactions were novel with respect to PKA signaling. The newly identified proteins are involved in many different aspects of cell signaling, metabolism, transport, growth, gene expression, etc. In addition, the identified proteins localize to various subcellular locations, including the cytoplasm,

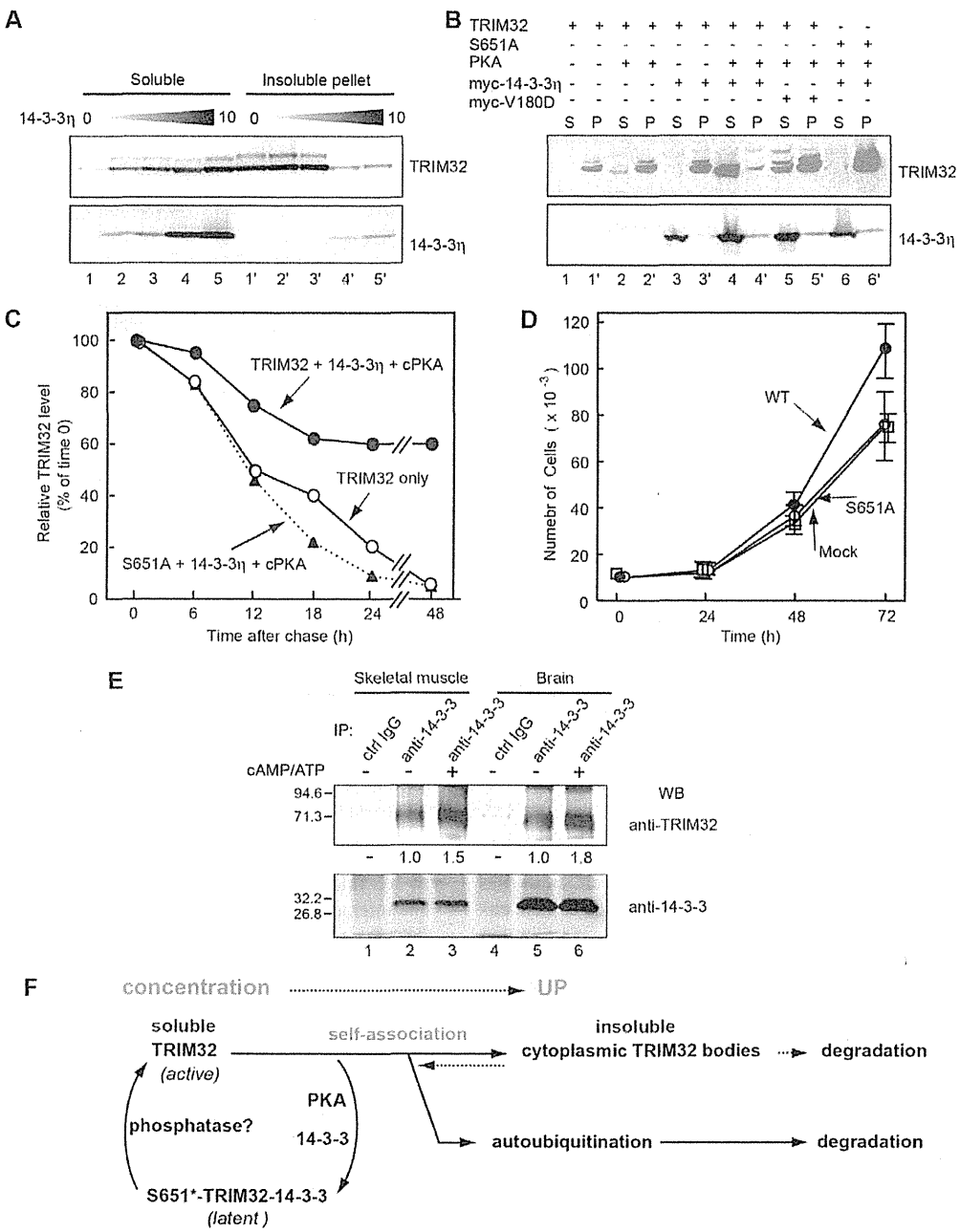

Fig. 6. 14-3-3/TRIM32 interaction is important for TRIM32 regulation. (**A**,**B**) 14-3-3–TRIM32 complex formation elevates the level of TRIM32 in the detergent-soluble fraction. HEK293 cells transiently transfected with the indicated expression plasmids (5 μg each) were lysed with 1% Triton X-100, and a soluble protein fraction was prepared by a 20-minute centrifugation at 9,000×g. The remaining insoluble pellet was solubilized in SDS-PAGE sample buffer. The cell lysates were analyzed by western blotting with monoclonal anti-FLAG and anti-14-3-3η as indicated. (**C**) 14-3-3 binding affects TRIM32 solubility. HEK293 cells were co-transfected with the indicated plasmids (5 μg each) and after 24 hours were incubated with cycloheximide (10 mM). Soluble proteins were extracted at the indicated times as in A and B and analyzed by western blotting with anti-TRIM32. Results were normalized to 1 at time 0 for each experiment and expressed as percentages. (**D**) 14-3-3 binding is necessary for the TRIM32-mediated acceleration of NIH3T3 cell growth. NIH3T3 cells infected with a retrovirus encoding FLAG–TRIM32 (WT), FLAG–S651A mutant (S651A) or the corresponding empty vector (Mock) were seeded at 1×10^4 cells in six-well plates and harvested for determination of the number of cells at the indicated times. Each value represents the mean ± s.d. of three experiments. (**E**) TRIM32 is co-immunopurified with 14-3-3 from mouse skeletal muscle and brain. Anti-PAN 14-3-3 (4 μg) or preimmune IgG (4 μg) were used for immunoprecipitation from 1% Triton X-100-solubilized mouse skeletal muscle (lanes 1–3) and brain extracts (lanes 4–6). The immunoprecipitates were subjected to non-reducing SDS-PAGE followed by WB with anti-TRIM32 (upper panel) or anti-PAN14-3-3 (lower panel). Exogenous cAMP (0.5 mM), ATP (0.5 mM) and magnesium chloride (10 mM) were added to the homogenates and incubated at 32°C for 20 minutes (lanes 3 and 6). The intensity of each TRIM32 band shown in the upper panel was also quantified by densitometry and expressed as fold change of the levels in non-stimulated homogenates. (**F**) Schematic illustration of the proposed role for 14-3-3 in regulation of TRIM32.

nucleus, cytoskeleton, mitochondria, endoplasmic reticulum and cell membrane. Previous genetic studies with yeast have pointed out that there may be many functional links between 14 and 3-3 and PKA signaling pathways (Gelperin et al., 1995; Roberts et al., 1997). Indeed, overexpression of *TPK1*, encoding the catalytic subunit of PKA, can partially suppress the lethality caused by depletion of Bmh (yeast homolog of 14-3-3) (Gelperin et al., 1995). Thus, the diversity of the protein complexes identified in our study complements the genetic proposal and further provides experimental evidence for a direct link between 14 and 3-3 and PKA in a wide range of cell functions.

Our results indicate that 14-3-3 binds TRIM32 directly when the ligase is phosphorylated by PKA at Ser651, located in the NHL domain. The NHL domain is a tryptophan-rich protein–protein interaction module, and indeed TRIM32 has been shown to interact with various substrates including Abi2 and with AGO1 through its NHL domain (Kano et al., 2008; Schwamborn et al., 2009). In the crystal structure of the NHL domain of brain tumor (Brat), a member of the RBCC-NHL family that lacks only the RING domain (Edwards et al., 2003), the NHL domain forms a six-bladed β-propeller, with the blades, consisting of the six individual NHL repeats, arrayed radially around a central shaft. Importantly, the top is mostly electropositive whereas the bottom is much more electronegative, and it has been proposed that the electropositive top surface may represent the ligand-binding face of NHL-containing proteins (Edwards et al., 2003). From this perspective, the interaction of TRIM32 with 14-3-3 reported here appears to be unique because this interaction occurred in response to phosphorylation of TRIM32 at Ser651 (Fig. 2), which is located in the C-terminal loop of the NHL domain exposed outside the propeller shaft and pointed toward the electronegative bottom side (Edwards et al., 2003). Furthermore, we indeed found that association of 14-3-3 with phosphorylated TRIM32 did not significantly affect the interaction of TRIM32 with Abi2 and AGO1 as analyzed by co-immunoprecipitation (supplementary material Fig. S5). Thus, 14-3-3 may represent a novel class of NHL-domain-binding proteins whose interaction inhibits TRIM32 enzymatic activity and CB formation in conjunction with PKA.

CBs may reflect the ability of TRIM proteins to self-associate and form large complexes (Song et al., 2005; Ganser-Pornillos et al., 2011). Because oligomerization and propensity to form large complexes appear to be common features of all TRIM members, these characteristics should be intrinsic to their functions. Kentsis et al. presented the 'scaffolding' model where TRIM oligomers could support the assembly of partner proteins and amplify or control specific enzymatic reactions (Kentsis et al., 2002). In the present study, we showed that 14-3-3 interaction specifically disrupted TRIM32 higher-order self-association without affecting dimerization and that this interaction repressed both TRIM32 ubiquitin ligase activity and CB formation (Figs 3–5). Thus, our results complement the scaffolding model suggested by Kentsis et al. and provide additional evidences that TRIM self-assembly may be critical for cellular TRIM functions (Kentsis et al., 2002). This finding is particularly relevant given the recent finding that a truncated dimer of TRIM5-21R that lacks the SPRY domain (domain equivalent to NHL of TRIM32) retains the capacity to form self-association-based hexagonal arrays, although with somewhat lower efficiency (Ganser-Pornillos et al., 2011). We assume that 14-3-3 binding may induce a conformational change or mask the NHL domain and possibly other parts of TRIM32 that is required for higher-order interaction of TRIM32 dimers once complex formation is triggered by phosphorylation at Ser651. Future structural studies will clarify the detailed molecular mechanism of the 14-3-3 interaction and the role of the NHL domain in the assembly of TRIM32 higher-order arrays.

Mounting evidence indicates that molecular chaperons such as Hsp90 and Hsp70 play important roles in the formation and/or maintenance of various cytoplasmic foci, including TRIM CBs, processing bodies, and stress granules (Hwang et al., 2010; Johnston et al., 2010). Importantly, the 14-3-3 family participates in the formation/maintenance of processing bodies (Okada et al., 2011) and stress granules (Stoecklin et al., 2004). These observations, together with our present results, suggest that 14-3-3 may have functional interplay with heat shock proteins, either cooperatively or separately, during formation of these cell structures. From this viewpoint, however, regulation by 14-3-3 appears to be unique because in most cases it requires phosphorylation for its interactions with other proteins and because it can modulate the activities of even mature enzymes and proteins in response to phosphorylation, although phosphorylation itself may promote unfolding of certain target proteins. From these results and other information (Vincenz and Dixit, 1996; Chen et al., 2003) we propose a potential role for 14-3-3 in PKA-dependent control of TRIM32 (Fig. 6F). Similar to many TRIM proteins, TRIM32 is distributed in the cytoplasm in both soluble and insoluble states, and the concentration of soluble TRIM32 is reduced by self-association-based autoubiquitylation and CB formation, depending on its expression levels (Locke et al., 2009). PKA phosphorylates soluble TRIM32 at Ser651; to be phosphorylated, however, TRIM32 must bind 14-3-3 to repress CB formation. Although 14-3-3 represses TRIM32 ligase activity, it may promote TRIM32 stability by blocking autoubiquitylation and thus degradation via the proteasome. Thus, 14-3-3 traps phosphorylated TRIM32 in a soluble and functionally latent complex upstream of autoubiquitylation and CB formation and drives the soluble–insoluble equilibrium of TRIM32 toward the soluble state by modulating the self-association-based protein–protein interactions (Fig. 6F). This regulatory mechanism should be reversible, as 14-3-3 interactions can be reversed by dephosphorylation (Dougherty and Morrison, 2004). This model is supported by our viral transduction experiment, which showed that the S651A mutant, which is enzymatically active yet unable to bind 14-3-3, could not facilitate NIH3T3 cell growth (Fig. 6D). We cannot exclude the possibility, however, that additional protein kinase(s) for TRIM32 could also phosphorylate Ser651 (or another site) to support 14-3-3 binding in these as well as other cell types.

In conclusion, we propose that 14-3-3 is a common cofactor for both the regulation of Nedd4-2 and TRIM32 through a PKA-dependent mechanism. In the past decade, many efforts have been made to identify specific TRIM32 substrates and to elucidate the mechanisms occurring in limb-girdle muscular dystrophy type 2H. The regulatory mechanism we describe here is the first and an important step toward understanding signaling pathways that may control TRIM32 functions at the molecular level. Because 14-3-3 binds many proteins – not only native but also denatured or misfolded proteins associated with several pathological processes – in response to phosphorylation, this regulatory mechanism may also have an important impact on

other 14-3-3-binding targets, especially aggregation-prone targets.

Materials and Methods

Materials

The mammalian expression plasmid carrying FLAG-tagged TRIM32 was generated by PCR using oligonucleotides 5′-CGGGATCCATGGCTGCAGCA-GCAGCTTC-3′ and 5′-CGGAATTCCTATGGGGTGGAATATCTTC-3′ and human TRIM32 cDNA (pOTB7, Funakosi) as template. The PCR fragment was digested with *Bam*HI and *Eco*RI and then inserted into the cloning site of the FLAG-tag vector pCMV-Tag2B (Invitrogen), termed pCMV-TRIM32. The expression plasmids for myc–14-3-3η and its V180D mutant or FLAG–14-3-3η have been described (Ichimura et al., 2005). The CFP-TRIM32 construct was created by ligating the *Bam*HI/*Eco*RI fragment of pCMV-TRIM32 into the *Bgl*II/*Eco*RI site of pECFP-C1 (Clontech). The deletion and point mutants of TRIM32 were created according to the standard protocol of PCR-based targeted mutagenesis (Ichimura et al., 2002). The 14-3-3η protein was prepared by cleavage of GST–14-3-3η (Nagaki et al., 2006) with Factor X (Bio-Rad). The catalytic subunit of PKA was isolated from porcine brain (Nagaki et al., 2006). Human TRIM32 was obtained from Abnova. The plasmids shown in supplementary material Fig. S1 were kind gifts from Drs Richard Roth (for AKT1S1–HA), Jennifer Byrne (for EGFP–TPD52L1), Daisuke Koya (for myc–Smurf1), and Danny Reinberg (for FLAG–RNF20) or were made by PCR using TORC2/pSport6 (kindly provided by Dr Yo Takemori, for FLAG–TORC2 in pCMV-Tag2B), pME18SFL3 (Toyobo, for FLAG–WDR20 in pCMV-Tag2B), pCMV-SPORT6 (Funakosi, for FLAG–TFEB in pCMV-Tag2B), or the reported plasmids of CaMKKα [(Ichimura et al., 2008) for myc–CaMKKα in pcDNA3], Nedd4-2 [(Ichimura et al., 2005) for myc–Nedd4-2 in pcDNA3], and TH [(Itagaki et al., 1999) for myc–TH in pcDNA3] as templates. The plasmid for FLAG–AGO1 was kindly provided by Dr Haruhiko Siomi. The PAN-14-3-3 antibody, anti-TRIM32, anti-GST and monoclonal anti-myc were purchased from Santa Cruz Biotechnology. Anti-14-3-3η was purchased from Immuno-Biological Laboratories. Polyclonal anti-myc and anti-phospho(Ser/Thr)-PKA substrate were purchased from Cell Signaling. Monoclonal anti-HA and anti-FLAG were purchased from Upstate and Kodak, respectively. Polyclonal anti-FLAG was purchased from Rockland. Monoclonal anti-tubulin was purchased from Sigma.

Quantitative proteomics

Quantitative proteomics was carried out as described previously (Ichimura et al., 2008). Six 15-cm dishes of PC12Mh cells (Ichimura et al., 2005) stably expressing MEF-fused 14-3-3 (η-isoform) were metabolically labeled with [^{13}C]Lys/Arg for 12 days. The labeled cells were stimulated with 50 μM forskolin (Sigma) for 20 minutes, lysed in 3 ml of lysis buffer [50 mM Tris-HCl, pH 7.5, 150 mM NaCl, 10% (w/v) glycerol, 100 mM NaF, 10 mM EGTA, 1 mM Na_3VO_4, 1% (w/v) Triton X-100, 5 mM $ZnCl_2$, 2 mM phenylmethylsulfonyl fluoride, 10 μg/ml aprotinin, and 1 μg/ml leupeptin] and combined with an equal volume of the lysate from unlabeled, non-stimulated PC12Mh cells. Proteins bound to the expressed MEF-14-3-3η were then purified from the combined lysates by the MEF method (Ichimura et al., 2005). The recovered proteins were digested with trypsin and then identified and quantified by two-dimensional liquid chromatography–tandem mass spectrometry using the MASCOT (Matrix Science) and STEM software programs (Shinkawa et al., 2005). For quantification, values were corrected by STEM for an incorporation efficiency of 81% [^{13}C]Lys and 70% [^{13}C]Arg.

Co-immunoprecipitation and pull-down assay

Co-immunoprecipitation analyses were conducted as described previously (Ichimura et al., 2005). HEK293 cells ($2–4\times10^6$) were transiently transfected with expression plasmids (each 5 μg) encoding FLAG–TRIM32 or its mutants, with or without myc–14-3-3 and cPKA. After 24 hours, the expressed FLAG–TRIM32 was immunoprecipitated with anti-FLAG–Sepharose (Sigma), washed five times with buffer A [50 mM Tris-HCl, pH 7.5, 150 mM NaCl, 10% (w/v) glycerol and 0.1% (w/v) Triton X-100], and the bound 14-3-3 was released from the beads with 1 mM synthetic phosphopeptide [LSQRQRSTS(*P*)TPNVHA, based on residues 250–265 of human cRaf1). Proteins were then separated by 10% SDS-PAGE and analyzed by western blotting using the specific antibodies indicated in each figure. For GST pull-down experiments, GST–TRIM32 or GST alone (each ~0.5 μg) was incubated with 14-3-3η (1 μg) for 20 minutes at 30℃ in 25 μl final volume (50 mM HEPES, pH 7.5, 10 mM magnesium acetate, and 0.1 mM ATP) in the presence or absence of 0.25 μl of the catalytic subunit of PKA. After incubation, glutathione–agarose beads (Pharmacia) were added to the reaction and further incubated for 60 minutes at 4℃. The beads were then washed five times with buffer A, and the precipitated complexes were analyzed by 10% SDS-PAGE followed by western blotting.

Immunopurification of 14-3-3 from mouse skeletal muscle and brain

Frozen mouse skeletal muscle and brain were homogenized in 10 volumes of lysis buffer, and the homogenates were centrifuged at 100,000 *g* for 30 minutes at 4℃. The cleared lysates (1.5 mg) were incubated with 4 μg of anti-PAN 14-3-3 IgG for 60 minutes at 4℃. Immobilized protein A/G–Sepharose (Santa Cruz Biotechnology) was added, and lysates were further incubated for 60 minutes at 4℃. Immunoprecipitated 14-3-3 complexes were washed five times with buffer A and eluted with SDS-PAGE sample buffer (lacking β-mercaptoethanol).

Immunofluorescence microscopy and electron microscopy

HEK293 cells grown on 3.5-cm plates (FluoroDish, World Precision Instruments, Inc.) were transfected with the indicated expression plasmids (each 0.5 μg) for 24 hours using Lipofectamine 2000 (Invitrogen). Transfected cells were rinsed with phosphate-buffered saline (PBS) containing 0.1 g/l $CaCl_2$ and 0.1 g/l $MgCl_2$ [PBS(+)] and fixed with 10% formalin in 70% PBS(+) for 30 minutes at 25℃. The fixed cells were washed four times with PBS, then incubated with 10% fetal bovine serum in PBS for 30 minutes at room temperature and subsequently incubated for 1 hour at room temperature with specific primary antibodies (see figure legends). After washing four times with PBS, the cells were incubated with Alexa-Fluor-488-conjugated (green) and Alexa-Fluor-594-conjugated (red) anti-rabbit or anti-mouse secondary antibodies (Molecular Probes) for 1 hour at room temperature. The stained cells were washed four times with PBS and then visualized using a Delta Vision microscope system (Applied Precision, Inc.).

For electron microscopy, HEK293 cells transfected with FLAG–TRIM32 were fixed for 1 hour at room temperature with 2.5% glutaraldehyde (TAAB Laboratories Equipment Ltd) in 0.1 M sodium phosphate buffer (pH 7.2), washed with PBS, and postfixed with 1% osmium tetroxide for 1 hour at room temperature in 0.1 M sodium phosphate buffer. Cells were then dehydrated with ethanol up to 100%, and finally embedded with Quetol 812-based resin (Nisshin EM). Ultrathin sections were stained with uranyl acetate and lead citrate and mounted on 150-mesh copper grids. Electron microscopy images were collected with a TEM H7100 (Hitachi Ltd) and scanned with a SUPER COOLSCAN 8000 (Nikon). Counting FLAG–TRIM32-expressing and myc–14-3-3-expressing cells revealed that the efficiency of FLAG–TRIM32 expression was 20–40% and that more than 90% of the FLAG–TRIM32-positive cells were also positive for myc-14-3-3 expression.

In-cell ubiquitylation assay

The ubiquitylation assay was performed as described previously (Ichimura et al., 2005). HEK293 cells ($2–4\times10^6$) were co-transfected with the indicated expression plasmids (each 5 μg) for 48 hours and lysed in 1% SDS. Samples were subsequently diluted with 9 volumes of lysis buffer and incubated with anti-FLAG–Sepharose beads (Sigma) or with anti-HA affinity matrix (Roche). The beads were washed five times with buffer A, and bound proteins were analyzed by 7.5% or 10% SDS-PAGE followed by western blotting with monoclonal anti-HA or anti-FLAG.

Sucrose density gradient

HEK293 cells ($2–4\times10^6$) were transfected with the indicated expression plasmids (each 5 μg) for 36 hours and homogenized in PBS. The homogenates (50 μg protein) were loaded on to a sucrose density gradient (5–20%, w/v) and centrifuged at 100,000 *g* for 18 hours at 4℃. The samples were fractionated from the bottom of the tubes, precipitated with 10% trichloroacetic acid, and subjected to 10% SDS-PAGE followed by western blotting with anti-TRIM32. The gel image was quantified with an E-Graph densitometer (ATTO) and the results were expressed as a percentage of total amounts of protein in each experiment.

Retroviral infection and cell counting

Retrovirus expression vectors for FLAG–TRIM32 wild-type (WT) and S651A point mutant (S651A) were constructed with pMX-puro (Kano et al., 2008). NIH3T3 fibroblasts were infected with retroviruses produced by Plat-E packaging cells as described previously (Kano et al., 2008). Infected cells were seeded at 1×10^4 cells per well in six-well plates and harvested for determination of cell number at various times.

Acknowledgements

We thank H. Siomi, R. Roth, J. Byrne, D. Koya, D. Reinberg and Y. Takemori for plasmids, and L. Greene for PC12 cells. We also thank S. Yamada, K. Kakiuchi, J. Yoshida, C. Uchida, K. Nishijima and Y. Komata for help in doing some experiments.

Author contributions

T.I. carried out most of the experiments. M.T., I.S., H.K. and T.I. helped with mass spectrometry and immunocytochemical analyses. T.S. and S.H. contributed in the generation of stable NIH3T3 cells. T.I. and N.H. evaluated experiments and wrote the manuscript. All authors were involved in data discussions and preparing the final version of the manuscript.

Funding

This work was supported by the Ministry of Education, Culture, Sports, Science and Technology of Japan through Grants-in-Aid for Scientific Research [grant numbers 21570213 to T.I.; 24112006 and 24390065 to S.H.]; the Integrated Proteomics System Project, Pioneer Research on Genome the Frontier; the Mitsubishi Pharma Research foundation; the Suhara Memorial Foundation; and the Sumitomo Foundation.

Supplementary material available online at
http://jcs.biologists.org/lookup/suppl/doi:10.1242/jcs.122069/-/DC1

References

Albor, A., El-Hizawi, S., Horn, E. J., Laederich, M., Frosk, P., Wrogemann, K. and Kulesz-Martin, M. (2006). The interaction of Piasy with Trim32, an E3-ubiquitin ligase mutated in limb-girdle muscular dystrophy type 2H, promotes Piasy degradation and regulates UVB-induced keratinocyte apoptosis through NFkappaB. *J. Biol. Chem.* **281**, 25850-25866.

Bhalla, V., Daidié, D., Li, H., Pao, A. C., LaGrange, L. P., Wang, J., Vandewalle, A., Stockand, J. D., Staub, O. and Pearce, D. (2005). Serum- and glucocorticoid-regulated kinase 1 regulates ubiquitin ligase neural precursor cell-expressed, developmentally down-regulated protein 4-2 by inducing interaction with 14-3-3. *Mol. Endocrinol.* **19**, 3073-3084.

Campbell, E. M., Dodding, M. P., Yap, M. W., Wu, X., Gallois-Montbrun, S., Malim, M. H., Stoye, J. P. and Hope, T. J. (2007). TRIM5 alpha cytoplasmic bodies are highly dynamic structures. *Mol. Biol. Cell* **18**, 2102-2111.

Chen, H. K., Fernandez-Funez, P., Acevedo, S. F., Lam, Y. C., Kaytor, M. D., Fernandez, M. H., Aitken, A., Skoulakis, E. M., Orr, H. T., Botas, J. et al. (2003). Interaction of Akt-phosphorylated ataxin-1 with 14-3-3 mediates neurodegeneration in spinocerebellar ataxia type 1. *Cell* **113**, 457-468.

Coblitz, B., Wu, M., Shikano, S. and Li, M. (2006). C-terminal binding: an expanded repertoire and function of 14-3-3 proteins. *FEBS Lett.* **580**, 1531-1535.

Diaz-Griffero, F., Li, X., Javanbakht, H., Song, B., Welikala, S., Stremlau, M. and Sodroski, J. (2006). Rapid turnover and polyubiquitylation of the retroviral restriction factor TRIM5. *Virology* **349**, 300-315.

Dougherty, M. K. and Morrison, D. K. (2004). Unlocking the code of 14-3-3. *J. Cell Sci.* **117**, 1875-1884.

Edwards, T. A., Wilkinson, B. D., Wharton, R. P. and Aggarwal, A. K. (2003). Model of the brain tumor-Pumilio translation repressor complex. *Genes Dev.* **17**, 2508-2513.

Fridell, R. A., Harding, L. S., Bogerd, H. P. and Cullen, B. R. (1995). Identification of a novel human zinc finger protein that specifically interacts with the activation domain of lentiviral Tat proteins. *Virology* **209**, 347-357.

Frosk, P., Weiler, T., Nylen, E., Sudha, T., Greenberg, C. R., Morgan, K., Fujiwara, T. M. and Wrogemann, K. (2002). Limb-girdle muscular dystrophy type 2H associated with mutation in TRIM32, a putative E3-ubiquitin-ligase gene. *Am. J. Hum. Genet.* **70**, 663-672.

Ganguly, S., Weller, J. L., Ho, A., Chemineau, P., Malpaux, B. and Klein, D. C. (2005). Melatonin synthesis: 14-3-3-dependent activation and inhibition of arylalkylamine N-acetyltransferase mediated by phosphoserine-205. *Proc. Natl. Acad. Sci. USA* **102**, 1222-1227.

Ganser-Pornillos, B. K., Chandrasekaran, V., Pornillos, O., Sodroski, J. G., Sundquist, W. I. and Yeager, M. (2011). Hexagonal assembly of a restricting TRIM5alpha protein. *Proc. Natl. Acad. Sci. USA* **108**, 534-539.

Gelperin, D., Weigle, J., Nelson, K., Roseboom, P., Irie, K., Matsumoto, K. and Lemmon, S. (1995). 14-3-3 proteins: potential roles in vesicular transport and Ras signaling in Saccharomyces cerevisiae. *Proc. Natl. Acad. Sci. USA* **92**, 11539-11543.

Hatakeyama, S. (2011). TRIM proteins and cancer. *Nat. Rev. Cancer* **11**, 792-804.

Horn, E. J., Albor, A., Liu, Y., El-Hizawi, S., Vanderbeek, G. E., Babcock, M., Bowden, G. T., Hennings, H., Lozano, G., Weinberg, W. C. et al. (2004). RING protein Trim32 associated with skin carcinogenesis has anti-apoptotic and E3-ubiquitin ligase properties. *Carcinogenesis* **25**, 157-167.

Hwang, C. Y., Holl, J., Rajan, D., Lee, Y., Kim, S., Um, M., Kwon, K. S. and Song, B. (2010). Hsp70 interacts with the retroviral restriction factor TRIM5alpha and assists the folding of TRIM5alpha. *J. Biol. Chem.* **285**, 7827-7837.

Ichimura, T., Wakamiya-Tsuruta, A., Itagaki, C., Taoka, M., Hayano, T., Natsume, T. and Isobe, T. (2002). Phosphorylation-dependent interaction of kinesin light chain 2 and the 14-3-3 protein. *Biochemistry* **41**, 5566-5572.

Ichimura, T., Yamamura, H., Sasamoto, K., Tominaga, Y., Taoka, M., Kakiuchi, K., Shinkawa, T., Takahashi, N., Shimada, S. and Isobe, T. (2005). 14-3-3 proteins modulate the expression of epithelial Na+ channels by phosphorylation-dependent interaction with Nedd4-2 ubiquitin ligase. *J. Biol. Chem.* **280**, 13187-13194.

Ichimura, T., Taoka, M., Hozumi, Y., Goto, K. and Tokumitsu, H. (2008). 14-3-3 Proteins directly regulate Ca(2+)/calmodulin-dependent protein kinase kinase alpha through phosphorylation-dependent multisite binding. *FEBS Lett.* **582**, 661-665.

Itagaki, C., Isobe, T., Taoka, M., Natsume, T., Nomura, N., Horigome, T., Omata, S., Ichinose, H., Nagatsu, T., Greene, L. A. et al. (1999). Stimulus-coupled interaction of tyrosine hydroxylase with 14-3-3 proteins. *Biochemistry* **38**, 15673-15680.

Johnston, M., Geoffroy, M. C., Sobala, A., Hay, R. and Hutvagner, G. (2010). HSP90 protein stabilizes unloaded argonaute complexes and microscopic P-bodies in human cells. *Mol. Biol. Cell* **21**, 1462-1469.

Kano, S., Miyajima, N., Fukuda, S. and Hatakeyama, S. (2008). Tripartite motif protein 32 facilitates cell growth and migration via degradation of Abl-interactor 2. *Cancer Res.* **68**, 5572-5580.

Kentsis, A., Gordon, R. E. and Borden, K. L. (2002). Control of biochemical reactions through supramolecular RING domain self-assembly. *Proc. Natl. Acad. Sci. USA* **99**, 15404-15409.

Kudryashova, E., Kudryashov, D., Kramerova, I. and Spencer, M. J. (2005). Trim32 is a ubiquitin ligase mutated in limb girdle muscular dystrophy type 2H that binds to skeletal muscle myosin and ubiquitinates actin. *J. Mol. Biol.* **354**, 413-424.

Kudryashova, E., Wu, J., Havton, L. A. and Spencer, M. J. (2009). Deficiency of the E3 ubiquitin ligase TRIM32 in mice leads to a myopathy with a neurogenic component. *Hum. Mol. Genet.* **18**, 1353-1367.

Kudryashova, E., Struyk, A., Mokhonova, E., Cannon, S. C. and Spencer, M. J. (2011). The common missense mutation D489N in TRIM32 causing limb girdle muscular dystrophy 2H leads to loss of the mutated protein in knock-in mice resulting in a Trim32-null phenotype. *Hum. Mol. Genet.* **20**, 3925-3932.

Li, X., Yeung, D. F., Fiegen, A. M. and Sodroski, J. (2011). Determinants of the higher order association of the restriction factor TRIM5alpha and other tripartite motif (TRIM) proteins. *J. Biol. Chem.* **286**, 27959-27970.

Locke, M., Tinsley, C. L., Benson, M. A. and Blake, D. J. (2009). TRIM32 is an E3 ubiquitin ligase for dysbindin. *Hum. Mol. Genet.* **18**, 2344-2358.

Nagaki, K., Yamamura, H., Shimada, S., Saito, T., Hisanaga, S., Taoka, M., Isobe, T. and Ichimura, T. (2006). 14-3-3 Mediates phosphorylation-dependent inhibition of the interaction between the ubiquitin E3 ligase Nedd4-2 and epithelial Na+ channels. *Biochemistry* **45**, 6733-6740.

Nisole, S., Stoye, J. P. and Saïb, A. (2005). TRIM family proteins: retroviral restriction and antiviral defence. *Nat. Rev. Microbiol.* **3**, 799-808.

Okada, N., Yabuta, N., Suzuki, H., Aylon, Y., Oren, M. and Nojima, H. (2011). A novel Chk1/2-Lats2-14-3-3 signaling pathway regulates P-body formation in response to UV damage. *J. Cell Sci.* **124**, 57-67.

Pertel, T., Hausmann, S., Morger, D., Züger, S., Guerra, J., Lascano, J., Reinhard, C., Santoni, F. A., Uchil, P. D., Chatel, L. et al. (2011). TRIM5 is an innate immune sensor for the retrovirus capsid lattice. *Nature* **472**, 361-365.

Reymond, A., Meroni, G., Fantozzi, A., Merla, G., Cairo, S., Luzi, L., Riganelli, D., Zanaria, E., Messali, S., Cainarca, S. et al. (2001). The tripartite motif family identifies cell compartments. *EMBO J.* **20**, 2140-2151.

Roberts, R. L., Mösch, H. U. and Fink, G. R. (1997). 14-3-3 proteins are essential for RAS/MAPK cascade signaling during pseudohyphal development in S. cerevisiae. *Cell* **89**, 1055-1065.

Ryu, Y. S., Lee, Y., Lee, K. W., Hwang, C. Y., Maeng, J. S., Kim, J. H., Seo, Y. S., You, K. H., Song, B. and Kwon, K. S. (2011). TRIM32 protein sensitizes cells to tumor necrosis factor (TNFα)-induced apoptosis via its RING domain-dependent E3 ligase activity against X-linked inhibitor of apoptosis (XIAP). *J. Biol. Chem.* **286**, 25729-25738.

Schwamborn, J. C., Berezikov, E. and Knoblich, J. A. (2009). The TRIM-NHL protein TRIM32 activates microRNAs and prevents self-renewal in mouse neural progenitors. *Cell* **136**, 913-925.

Shinkawa, T., Taoka, M., Yamauchi, Y., Ichimura, T., Kaji, H., Takahashi, N. and Isobe, T. (2005). STEM: a software tool for large-scale proteomic data analyses. *J. Proteome Res.* **4**, 1826-1831.

Song, B., Diaz-Griffero, F., Park, D. H., Rogers, T., Stremlau, M. and Sodroski, J. (2005). TRIM5alpha association with cytoplasmic bodies is not required for antiretroviral activity. *Virology* **343**, 201-211.

Stoecklin, G., Stubbs, T., Kedersha, N., Wax, S., Rigby, W. F., Blackwell, T. K. and Anderson, P. (2004). MK2-induced tristetraprolin:14-3-3 complexes prevent stress granule association and ARE-mRNA decay. *EMBO J.* **23**, 1313-1324.

Urano, T., Saito, T., Tsukui, T., Fujita, M., Hosoi, T., Muramatsu, M., Ouchi, Y. and Inoue, S. (2002). Efp targets 14-3-3 sigma for proteolysis and promotes breast tumour growth. *Nature* **417**, 871-875.

Vincenz, C. and Dixit, V. M. (1996). 14-3-3 proteins associate with A20 in an isoform-specific manner and function both as chaperone and adapter molecules. *J. Biol. Chem.* **271**, 20029-20034.

Yokota, T., Mishra, M., Akatsu, H., Tani, Y., Miyauchi, T., Yamamoto, T., Kosaka, K., Nagai, Y., Sawada, T. and Heese, K. (2006). Brain site-specific gene expression analysis in Alzheimer's disease patients. *Eur. J. Clin. Invest.* **36**, 820-830.

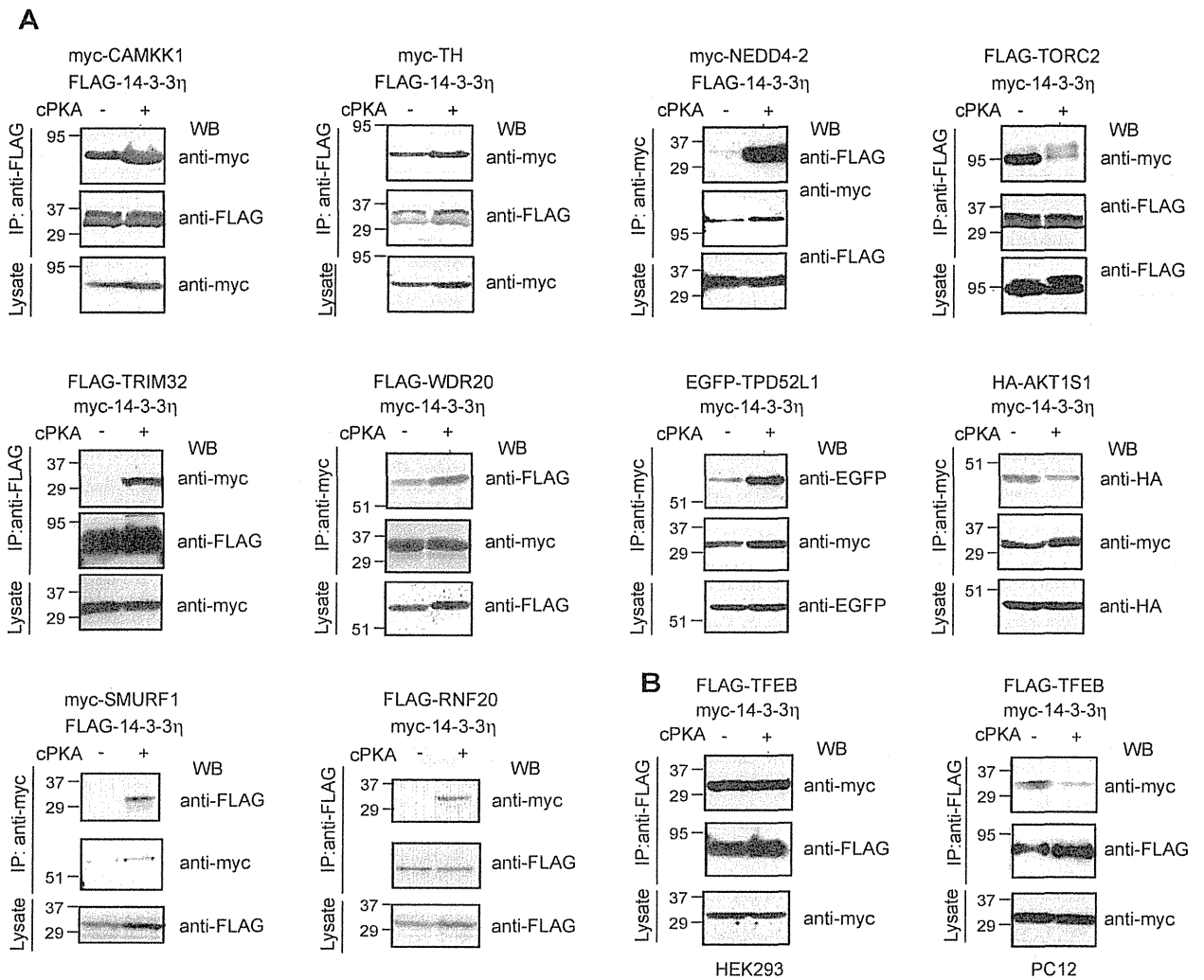

Fig. S1. Regulation of 14-3-3 interactions by cPKA. (A) HEK293 cells were transfected with the indicated plasmids with (+) or without (–) cPKA (5 μg each). After 24 h, the expressed proteins were immunoprecipitated (IP) with anti-FLAG or anti-myc, and the immunocomplexes were analyzed by 10% SDS-PAGE followed by western blotting (WB) with the indicated antibodies (top and middle panels, respectively). The cell lysates (20 μg of protein each) were also analyzed by WB to determine protein levels of co-precipitated proteins (bottom panels). Molecular size markers, in kDa, are indicated to the left. (B) HEK293 cells (left panels) or PC12 cells (right panels) were co-transfected with the indicated constructs and analyzed by WB as in panel A.